First large capsule implosions in a frustum-shaped *hohlraum* ⊘

K. L. Baker ✉ iD ; P. A. Amendt iD ; J. S. Ross iD ; V. A. Smalyuk; O. L. Landen iD ; D. D. Ho iD ; S. Khan iD ;
S. W. Haan iD ; J. D. Lindl iD ; D. Mariscal iD ; J. L. Milovich iD ; S. MacLaren iD ; Y. Ping iD ; D. J. Strozzi iD ;
R. M. Bionta iD ; D. T. Casey iD ; P. M. Celliers iD ; D. N. Fittinghoff iD ; H. Geppert-Kleinrath;
V. Geppert-Kleinrath iD ; K. D. Hahn iD ; M. Gatu Johnson iD ; Y. Kim iD ; K. Meaney iD ; M. Millot iD ;
R. Nora iD ; P. L. Volegov iD ; C. H. Wilde iD

Check for updates

View Online

Export Citation

CrossMark

First large capsule implosions in a frustum-shaped *hohlraum*

View Online   Export Citation   CrossMark

K. L. Baker,[1,a)] [iD] P. A. Amendt,[1] [iD] J. S. Ross,[1] [iD] V. A. Smalyuk,[1] O. L. Landen,[1] [iD] D. D. Ho,[1] [iD] S. Khan,[1] [iD]
S. W. Haan,[1] [iD] J. D. Lindl,[1] [iD] D. Mariscal,[1] [iD] J. L. Milovich,[1] [iD] S. MacLaren,[1] [iD] Y. Ping,[1] [iD] D. J. Strozzi,[1] [iD]
R. M. Bionta,[1] [iD] D. T. Casey,[1] [iD] P. M. Celliers,[1] [iD] D. N. Fittinghoff,[1] [iD] H. Geppert-Kleinrath,[2] V. Geppert-Kleinrath,[2]
[iD] K. D. Hahn,[1] [iD] M. Gatu Johnson,[3] [iD] Y. Kim,[2] [iD] K. Meaney,[2] [iD] M. Millot,[1] R. Nora,[1] [iD] P. L. Volegov,[2] [iD]
and C. H. Wilde[2] [iD]

AFFILIATIONS

[1]Lawrence Livermore National Laboratory, Livermore, California 94550, USA
[2]Los Alamos National Laboratory, Los Alamos, New Mexico 87544, USA
[3]Massachusetts Institute of Technology, Cambridge, Massachusetts 02139, USA

[a)]Author to whom correspondence should be addressed: baker7@llnl.gov

ABSTRACT

We report on the first indirect-drive implosions driven by a dual conical frustum-shaped *hohlraum* denoted "frustraum" and the experimental tuning campaigns leading up to two layered implosions. The campaign used 1.2 and 1.4 mm inner radius high density carbon (HDC) capsules and represented the largest HDC capsules to be imploded on the National Ignition Facility via indirect drive. Several techniques were successfully implemented to control the Legendre mode 2 capsule symmetry of the implosions, including changing the wall angle of the frustraum, which is not possible with cylindrical *hohlraums*. A mode 4 feature was observed and its implications for hotspot mix discussed. Two layered implosions were conducted with 1.2 mm inner radius capsules, the latter of which achieved the highest layered capsule absorbed energy on the National Ignition Facility using only 1.74 MJ of laser energy. The layered implosion results, along with generalized Lawson parameters, suggest that increasing the energy absorbed by the capsule at the expense of long coast times makes it more challenging to achieve ignition and that further reducing coast time (time between end of laser pulse and bang time) closer to the 1 ns level is warranted to improve the areal density and make it easier to achieve the hotspot temperature, alpha heating, and yield amplification required for ignition.

I. INTRODUCTION

In indirect drive inertial confinement fusion (ICF) at the National Ignition Facility (NIF), a deuterium–tritium (DT) filled capsule[1,2] is driven by the ablation pressure from x rays at peak radiation temperatures Tr of around 300 eV. These x rays are produced by irradiating the inside of a high-Z *hohlraum* with 192 laser beams entering through two laser entrance holes (LEHs) on either end. The DT hotspot must reach high ion temperatures, $T_{ion} > 5$ keV, and high areal densities, $\rho r > 0.2$–0.3 g/cm^2, to initiate thermonuclear burn, and the total yield depends on the confinement time provided by the total areal density of the DT and remaining ablator, typically designed at 1–2 g/cm^2.

The goal of the NIF is to increase the liberated fusion energy in ICF experiments well past the ignition threshold and the input laser energy. Most recent ICF efforts have focused on increasin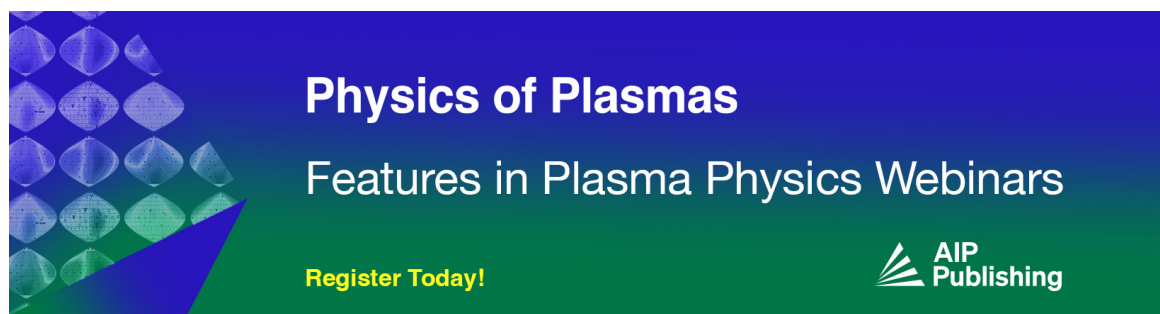g the capsule size to increase the capsule absorbed energy[3–7] and this paper follows in this vein using a frustraum[8] to drive a 1.2 mm inner radius high

density carbon (HDC) capsule and setting the record for the maximum capsule absorbed energy achieved on the NIF for laser energies less than 2.05 MJ. Recent experiments with 1.05 mm HDC capsules at 2.05 MJ have surpassed this capsule absorbed energy seen in the frustraum at 1.7 MJ of laser energy (N210725). This large capsule size in a relatively large frustraum, however, results in longer coast times, >1.5 ns, which limits the performance of the implosions.

In Sec. II, we review the experimental parameters from the frustraum campaign. This campaign used a frustraum *hohlraum* that measured 9.76 mm in diameter at the capsule equator by 12.24 mm in length with 23° wall angles to drive most of the implosions. In Sec. III, we discuss the experiments conducted to test several methods to control the capsule symmetry in preparation for cryogenically layered implosions. The layered implosions on the NIF contain a thin cryogenic deuterium–tritium (DT) ice layer, 40–65 μm thick, on the inside of the capsule with a very low vapor density of DT, $\sim$0.44 mg/cm^3,

28 September 2023 14:55:57

internal to the ice layer. This differs from symmetry capsules, which use a gas fill internal to the ablator at densities of $\sim$4 mg/cm^3 without an ice layer. In Sec. IV, we discuss the two layered implosions carried out in the frustraum platform. We compare the frustraum to the other cylinder *hohlraum* campaigns, which use HDC ablators on the NIF to better understand the effects of capsule absorbed energy, dopant level, and coast time on the performance of these implosions. We also derive generalized Lawson criteria, which enable us to define a minimum yield and ion temperature as a function of coast time necessary to reach ignition and indicate how far these frustraum-driven implosions are from reaching ignition. In Sec. V, we summarize the results of this Frustraum platform and describe potential improvements to increase the performance of this platform in the future.

II. EXPERIMENTAL DETAILS

The *hohlraum* configuration used in the experiments described in this article was a frustraum[8] geometry, as shown in Fig. 1. The frustraum used to drive these experiments, in all but one experiment, measured 9.76 mm in diameter at the capsule equator and was 12.24 mm in length. These *hohlraums* were built with 23° wall angles with a wall area $A_{wall} = 270$ mm^2 and had a laser entrance hole (LEH) that was 3.1 mm in diameter on either end of the frustraum. The wall area for this frustraum is slightly larger than the 6.4 mm diameter by 11.24 mm long cylindrical *hohlraum* used in the HyE campaigns, $A_{wall} = 257$ mm^2. The wall material for the *hohlraums* was gold at lower laser energies and gold-lined uranium at higher laser energies. The HDC capsules placed in the center of the frustraum had an inner radius of 1.2 mm and an overall shell thickness of $\sim$81 μm. The capsules consisted of a clean HDC layer on the inside of the shell followed by a doped layer which contained 0.35% tungsten (W) dopant. The outer layer of the shell was again composed of clean HDC material. The symmetry and 2D-ConA experiments described below primarily
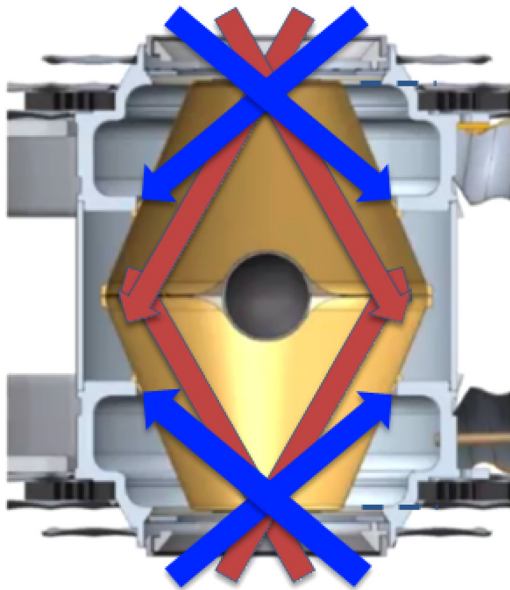
FIG. 1. Drawing of the frustraum used on the NIF. It consists of two conical frustum-shaped *hohlraums* joined together along the equator of the capsule.

used capsules that were filled with deuterium at 1817 Torr or a mixture of 67%/33% D^{3}He at 2164 Torr to give an initial mass density inside the capsule of 4 mg/cm^3 at the fielding temperature of 32 °K. The layered implosions used 5 μm fill tubes with 45 nm thick tents to hold the capsule in the target. In all cases, the frustraums were filled with 0.3 mg/cm^3 of ^{4}He gas. The implosions were driven by a three-stage laser pulse shape that generated three primary levels of x-ray drive in the *hohlraum* and, therefore, x-ray ablation pressure on the capsules, sending three primary shocks into the HDC ablator.

III. SYMMETRY CONTROL EXPERIMENTS
A. Legendre P2 mode sensitivity

Experiments were conducted to determine the sensitivity of the platform to various methods used to control the Legendre P2 mode asymmetry.[9] These experiments were designed using the Lasnex radiation hydrodynamics code.[10] One technique for controlling P2 is to adjust the inner beam cone fraction, defined as the energy in the inner cones divided by the total laser energy. While this technique is most useful in the first, foot, and second stage of the laser pulse, it can be used in the third stage, at peak laser power; however, it can prevent full delivery of the laser energy to the target when it is used at peak power and the inner and outer beams are on for the same duration. Thus, we conducted experiments to test other methods to control the capsule drive symmetry in the peak of the laser pulse, which included changes in the wavelength separation between the inner and outer beam cones, outer beam pointing, and the angle of the frustraum wall.

1. Wavelength separation between the inner and outer cones

One technique that is commonly used to change the P2 drive asymmetry for implosions on the NIF is to change the wavelength between the inner and outer beams,[11] which changes the level of cross beam energy transfer (CBET) between the beam cones. To move more energy from the outer beams to the inner beams, the wavelength of the inner beams is typically set to a longer wavelength than the outer beams. As the wavelength difference is increased, more energy is transferred from the outer cones to the inner cones and the drive at the equator of the capsule is increased, making the P2 mode capsule shape more positive. To determine the sensitivity of this method for controlling the P2 mode in the frustraum, a pair of implosion experiments were conducted, N200108 and N211017, with a change in the wavelength between the inner and outer beams. N200108 had the same wavelength on both the inner and outer beams and measured the hotspot shape at the implosion's stagnation time. N211017 had a wavelength separation of 0.5 Å between the inner and outer beams and this experiment radiographed the ablator shell as it was imploding, as well as measuring the hotspot shape at the implosion's stagnation time. This wavelength separation is at 1-omega, approximately 1053 nm, before frequency tripling of the laser beam. As shown in Fig. 2, P2 increased from -1 to 24 μm with the application of 0.5 Å longer wavelength on the inners. Both of these two experiments had the same average stagnated radius P0 = 83 μm. Taking into account the differences in inner beam cone fraction at peak power, the measured P2 sensitivity was $\sim$44 μm/Å. One other difference between the two experiments was that N211017 used a gold-lined depleted uranium (DU) frustraum and N200108 used a gold frustraum. These configurations behave the
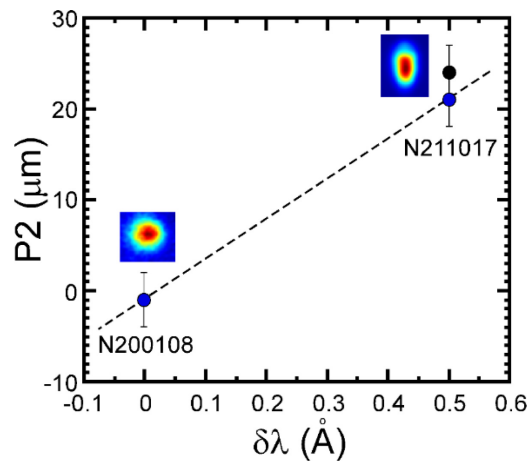
FIG. 2. Effect of a change in delta lambda, 0 (N200108)–0.5 Å (N211017), between the inner and outer cones on the P2 mode of the hotspot shape from neutron imaging. The black points represent the raw data and the blue points represent a correction due to the measured hotspot velocity.

FIG. 3. Effect of an outer beam pointing change, on the P2 mode of the hotspot shape from neutron imaging. (a) shows a change in where the 50° beams hit the wall as the pointing is changed. (b) Plot of the P2 from a 0.1 mm pointing change in the outer 44.5° and 50° cones between the pair of shots, N200721 and N201018, and a 0.2 mm pointing change in the outer 44.5° and 50° cones between the pair of shots, N200217 and N200108.

same in the first, foot, and second stages of the laser pulse, but the gold-lined DU frustraum reaches a higher effective peak power, ∼6.5%, due to the higher wall albedo when the Marshak wave breaks through the 700 nm thick gold liner. Comparison experiments in the previous BigFoot campaign, however, indicated that there was no meaningful change in the hotspot Legendre P2 mode between gold (N180128) and gold-lined DU (N180930) *hohlraums*. Simulations indicate that gold-lined DU *hohlraums* can result in a slightly more prolate implosion, few micrometers, compared to the same shot in a gold *hohlraum*. That would be in the direction of reducing the measured 44 μm/Å by 4–6 μm/Å.

2. Outer cone pointing change

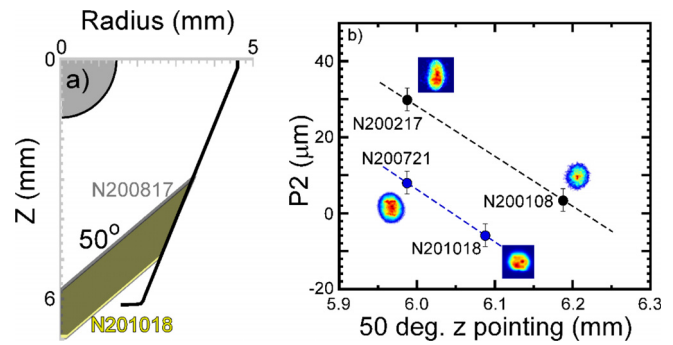Another technique that has been successful in changing P2 in cylindrical *hohlraums* is to change the outer beam pointing as shown in Fig. 3(a). Moving the outer beams closer to the capsule makes the P2 mode capsule shape more positive and moving it closer to the LEH to makes it more negative. To determine the sensitivity of this method of controlling P2 in the frustraum, two pairs of implosions were conducted. Between the experiments N200108 and N200217, a change in the outer beam pointing of 200 μm in z (along the frustraum axis) was made. In another set of experiments, N200721 and N201018, a change in the outer beam pointing of 100 μm in z was made. Figure 3(b) shows the hotspot shapes for N200108 and N200217, which both used the same laser pulse shape, symmetry platform, wavelength, and frustraum wall material. Taking into account changes in the inner beam cone fraction, this pair of experiments resulted in a P2 change of 24 μm or ∼12 μm/100 μm of pointing change in the outer beams.

Figure 3(b) also shows the hotspot shapes for N200721 and N201018, which both used the same laser pulse shape, symmetry platform, and frustraum wall material. One difference in this pair was that N201018 had a 0.4 Å shift between the 44.5° and 50° cones with the inner beams set to the average of these two wavelengths. The reason for this is that in the majority of the campaigns on the NIF the highest

levels of stimulated Brillouin scattering (SBS) are driven by the 50° outer cones. This SBS can be mitigated by imposing a small wavelength difference between the two outer cones, typically, 0.4 Å, which transfers energy from the 50° outer cones to the 44.5° outer cones to reduce the SBS levels on the 50° beams and increase it slightly on the 44.5° beams.[12] This wavelength change was applied as the laser energy was increased to ensure that the platform could reach high laser energies without driving damaging levels of SBS, >1 J/cm^2. Taking into account changes in the inner beam cone fraction, this pair of experiments resulted in a P2 change of 7 μm/100 μm pointing change in the outer beams. The four color wavelength present in N201018, however, made this experiment slightly more prolate than it otherwise would have been such that this latter pair of experiments is also consistent with a pointing change sensitivity of 10 to 12 μm/100 μm pointing change in the outer beams.

3. Wall angle change

Another technique that can be used in a frustraum to change the Legendre P2 mode is to alter the angle of the walls themselves. To determine the sensitivity of this method of controlling the Legendre P2 mode in the frustraum, a pair of implosions were conducted, N210608 and N210724, with a change in the wall angle of the frustraum between the two shots. The geometry for the experiments is shown in Fig. 4(a) with N210608 and N210724 performed in frustraums with a 23° (red) and 25° (black) wall angle, respectively. The increase in wall angle reduces the intensity of the outer beams on the wall by ∼12% reducing the gold bubble velocity. It also moves the outer beam spots closer to the midplane and at a larger radius, providing more drive to the capsule equator. The effective pointing change in the outer beams for the two degree increase in the wall angle is −0.13 mm in z and +5° in spot angle subtended to capsule with respect to the laser axis. The increase in wall angle also changes the plasma flow direction from the wall, which is then predicted to increase the cross-beam-energy-transfer from the outer to inner beams for the case of a positive $\Delta\lambda$. As seen in Fig. 4, increasing the wall angle by 2° increased the core P2 measured from neutron imaging by 45 μm. The ΔP2 has been corrected by −15 μm for a known mode 1
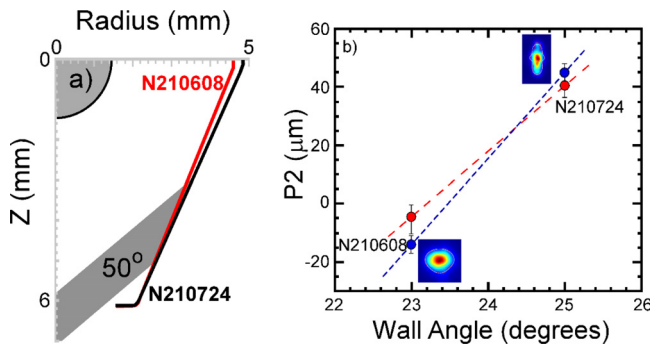
FIG. 4. Effect of a frustraum wall angle change on the P2 mode of the hotspot shape from neutron imaging. (a) Schematic showing the wall angle change from 23° (N210608) to 25° (N210724). (b) Plot of the measured P2 vs wall angle (blue) and P2 vs wall angle (red) corrected for hotspot motion for a measured hotspot vector of 130 km/s, $\theta = 109$, $\phi = 239$ for N210608 and 144 km/s, $\theta = 139$, $\phi = 266$ for N210724.

residual hotspot velocity on each of the shots. From Sec. III A 2, the -0.13 mm pointing change would represent a modest change in P2, $+16\,\mu m$, with the remaining $+29\,\mu m$ attributed to reduction in impairment of inner beam transport by the gold bubble from the reduced fluence on the wall and an increase in CBET.

4. Empirical mode P2 sensitivity

Previous papers have used empirical models to characterize and predict the P2 shape in cylindrical *hohlraums*.[13,14] A series of 14 experiments measuring shape were carried out in different frustraum configurations, which included wall angles of 21°, 23°, and 25°, diameters at the equator of the capsule of 7, 9.26, and 9.76 mm and capsule inner radii of 1050, 1200, and 1400 μm, In a similar fashion to cylindrical *hohlraum* empirical models, we have placed the 14 frustraum experiments in a similar plot with the P2 at 33% cone fraction along the y axis and the expression sqrt$(E_{out}/A/\rho)^{0.5}(\tau/R_{hohl})^2(CCR)^{0.5}$ along the x-axis as shown in Fig. 5. Here, E_{out} is the energy in the picket of the outer beams, A is the area of the outer beams, ρ is the density of the *hohlraum* gas, and τ is the time between the beginning and the middle of the peak power of the outer beam. R_{hohl} is the radius, where the 50° beams intersect the frustraum wall, and CCR is the minimum case-to-capsule ratio, the outer radius of the capsule, r_{cap}, divided by the closest radius of the frustraum to the capsule surface. The y value is calculated using the measured P2 (μm) and then subtracting off the changes in P2. The first change subtracted off is due to the peak cone fraction difference from 33%, $-100^*(0.33 - CF)^*3.5$. Another change in P2 is due to cross beam energy transfer between the inner and outer cones, $-(\delta\lambda$ in A$)^*38\,\mu m/A$. In this empirical model, we assume that there is no change in P2 due to the four color delta lambda (wavelength difference between the outer cones) but only from the two color delta lambda (wavelength difference between inners and average of the outers). The final change in the P2 is due to the outer beam spot motion from the initial average outer beam spot angle, θ_{init}, to the average outer beam spot angle at peak power, θ_{pp}, $-6.5(\theta_{pp} - 48.6°)$. For this latter change, we assume that the walls are moving radially inward at $\sim 71\,\mu m/ns$ and the value of 48.6° is just used to move all of the data points along the y axis. Similar to the empirical plot for
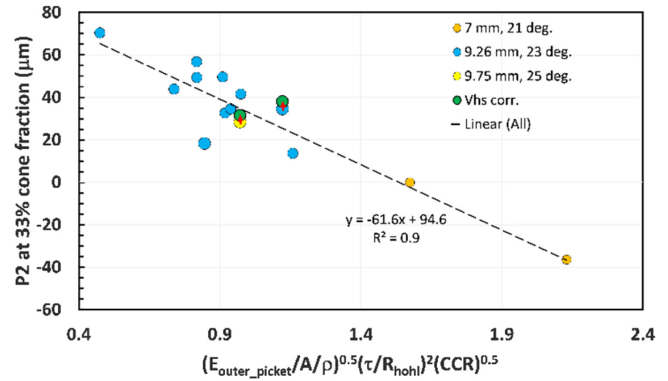
FIG. 5. Symmetry plot of the x-ray P2 shape in experiments conducted in the frustraum platform through calendar year 2021. These experiments include three different capsule inner radii, 1050, 1200, and 1400 μm; three wall angles 21°, 23°, and 25°; and three frustraum equatorial diameters, 7, 9.26, and 9.75 mm. A correction of the P2 shape due to the hotspot motion for two of the experiments is shown as the green circles with the red arrows showing the change in P2. The bubble size is proportional to the inner radius of the ablator capsule to the fifth power.

cylindrical *hohlraums*, most points fall along a line in this phase space for the frustraum experiments.

5. Smoothing effects of the large case-to-capsule ratio

The frustraum has a larger diameter at the equator than cylindrical *hohlraums* and, thus, perturbations on the wall are smoothed relative to cylinder due to the smaller solid angle of the perturbation on the capsule. This effect can be examined by comparing the perturbation caused by the two uncoated diagnostic windows in convergent ablator experiments that were carried out in each platform on the NIF. The windows are uncoated HDC, $800 \times 800\,\mu m^2$ in size and placed 180° apart on the *hohlraum* wall. These two windows cause an M2 mode to be generated on the capsule implosion, as viewed from the pole, due to the local reduction in the x-ray drive along the axis of the two diagnostic windows. Beam delivery is also a source of M2 but random M2 for this mechanism is expected to be $<0.2\%$ from beam balance. Figure 6(a) shows a plot of the hotspot M0 vs the initial capsule
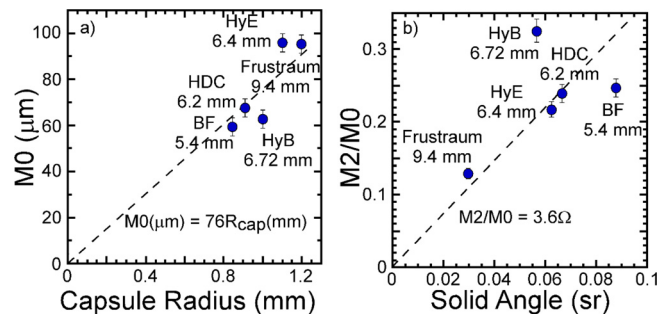
FIG. 6. (a) Hotspot radius, M0, vs the initial capsule radius showing similar compression ratios. (b) Capsule mode M2/M0 perturbation caused by to two 800 μm square uncoated 2D-ConA windows at the equatorial *hohlraum* wall, at phi angles of 78.75° and 258.75°, for different campaigns on the NIF as a function of the solid angle of the windows from the capsule.

radius for several platforms. The frustraum is represented by the 1200 μm inner radius point. Figure 6(b) shows the M2/M0 of the hotspot caused by the window perturbation as a function of the initial solid angle of the window on the capsule. The frustraum represents the smallest M2/M0 perturbation on the capsule due to its large CCR. There is roughly a linear effect with window solid angle on capsule hotspot M2/M0.

B. Reduction in systematic mode 1 perturbations in the *hohlraum*

Mode 1 also degrades the performance of layered implosions and has numerous sources.[15,16] These sources include a mode 1 driven by the as delivered laser energy or beam pointing, mode 1 variations in the capsule and ice thickness, and a capsule displaced from the *hohlraum* center.[17] Until recently, most layered implosions were carried out in *hohlraums* with diagnostic windows, which introduced a systematic mode 1 in all of these implosions. The second frustraum layered implosion, N210725, incorporated three diagnostic windows into the *hohlraum* with the placement of the windows in azimuth chosen to mitigate this systematic mode 1 perturbation that had been present in previous layered implosions. The windows are located at (90, 83.88), (90, 213.75), and (90, 315), roughly 120° apart from one another.

C. P4 effects

The experimental x-ray self-emission images from symmetry capsule, symcap, experiments show a feature that is reminiscent of the tent features seen in implosions with glow discharge plasma (GDP) capsules.[18–20] Integrated simulations with the tent included can reproduce the features seen in the experiments;[21] however, these features are also seen in *hohlraum* simulations with no tent present, though reduced relative to the experiments and the simulations including the tent. For these experiments, the z pointing of the 44.5° cone was further away from the capsule than the 50° cone, which increased the P4 in these experiments. In simulations, this feature is due to a coupling between the tent and a P4 mode driving the capsule in combination with a higher growth factor in the design. The top of Fig. 7 shows images of the hotspot as a function of time with time progressing from left to right. In these images, we see the propagation of two lines on the top and bottom of the hotspot penetrating further into the hotspot as a function of time. The outer edge of the hotspot provides a measure of the hotspot x-ray M0, from which we can deduce the center of the hotspot and the distance between the center of the hotspot and the leading edge of emission attributed to the P4/tent feature. The time dependences of the radius are plotted in Figs. 7(b) and 7(c), where the radius is the distance from the center of the hotspot to the inner radius of either line on the top and bottom. We can then use models to reproduce the experimental observations of the motion of the P4 feature into the hotspot and infer the mass injected into the hotspot from these P4 features. We implemented two models to reproduce the P4 feature trajectory through the hotspot and in both models make the simplifying assumption that the injected mass and cross-sectional area are not changing with time and the hotspot density is uniform inside the hotspot but varies in time. The first model is a snow-plow model that can be expressed by the following equation:

$$M_s V_s = (M_s + \beta\rho(t)Az(t))\frac{dz(t)}{dt}, \qquad (1)$$

where β is a parameter that allows some of the mass to not be accumulated, ρ is the hotspot density, A is the area of the injected jet, M_s is the initial mass of the injected jet, V_s is the initial velocity of the injected jet, and z is the position of the edge of the jet relative to the center of the hotspot. The time-dependent mass of the jet feature is given by $M_s + \beta\rho(t)Az(t)$, where M_s is the initial mass and $\beta\rho(t)Az(t)$ is the additional accumulated mass. The only time-dependent quantities in
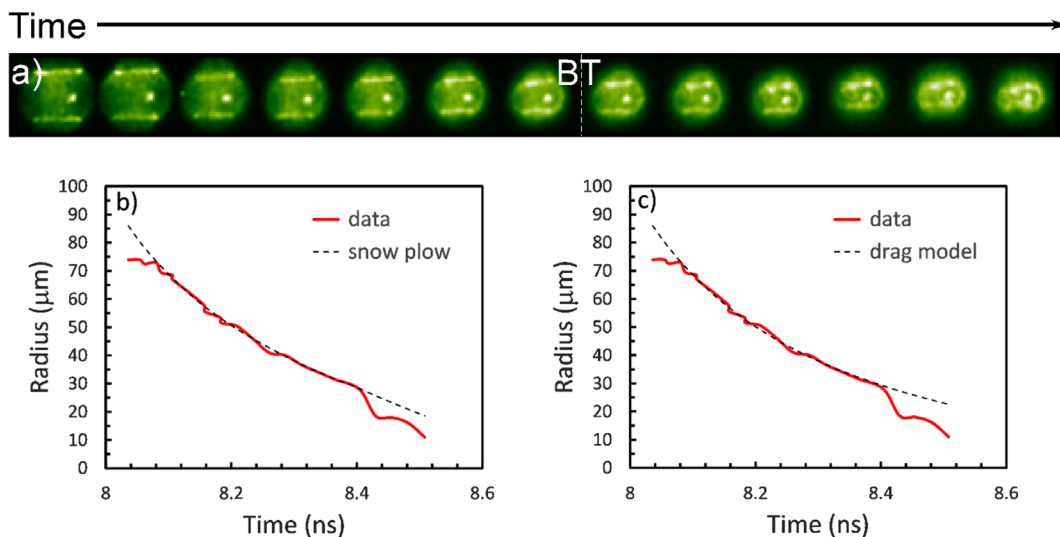
FIG. 7. Images of the x-ray hotspot shape as a function of time for the symmetry capsule experiment N201018 are shown in (a). The images show two bright ∼horizontal lines converging toward the axis along with a bright feature injected into the hotspot from the fill tube. The mass attributed to the line features is estimated using both a snow plow model (b) and a drag model (c).

this equation are ρ and z with the initial value of z(t_{init}) = 0 and the initial value of $\frac{dz}{dt}(t_{init}) = V_s$. The only change from a traditional snow-plow model[22,23] is the addition of the β term that allows only a portion of the hotspot mass to be swept up given that the time over which the feature travels through the hotspot is larger than its cross-sectional radius divided by the sound speed. The total accumulated mass in this model is then given by $\beta\rho A\Delta r$, where Δr is the distance traveled through the hotspot. The second model is a drag model, which can be expressed by the following equation:[23,24]

$$M_s\frac{dV_s}{dt} = C_D A\rho V_s^2/2, \qquad (2)$$

where M_s is the initial mass, V_s is the velocity of the horizontal feature, A is the area of the jet, ρ is the mass density of the hotspot, and C_D is the drag coefficient slowing down the jet of material. The hotspot density is changing rapidly as the hotspot is being compressed by the ablator and it can be fit with a simple polynomial, $\rho = \rho(0) + Bt + Dt^2$, to enable an analytic form for the velocity of the feature in the hotspot

$$V_s(t) = V_s(0)/(1 - C_D A V_s(0)(\rho(0)t + 0.5Bt^2 + 0.33Dt^3)/(2\,M_s)). \qquad (3)$$

Other models have been developed to infer the level of high-Z material mixed into the hotspot of layered implosions.[25] This model measures the total level of mix into the hotspot and assumes all of the x-ray emission comes from the hotspot. As such this model is not typically used for symcap implosions as discussed in this article where the majority of the x-ray emission can come from the ablator. Likewise this model assumes that the mix is in thermal equilibrium with the hotspot which recent work has disputed.[26] The models presented in this paper do not rely on whether the mix is in thermal equilibrium with the hotspot, whether the x-ray emission is only coming from the hotspot and not the ablator, they do not require nuclear yield data and they can look directly at the mix entering the hotspot from the feature causing the mix.

Both the snow plow and drag models were applied to the data in the top row of Fig. 7 to determine the quantities, A, M_s, V_s, r(t), and ρ(t) in Eqs. (1) and (2). These values of the parameter β in the snow-plow model and C_D in the drag model used in Figs. 7(b) and 7(c) were

$\beta = 0.44$ and $C_D = 1$. The snow-plow model is shown by the dashed black line in Fig. 7(b) and the drag model is shown by the dashed black line in Fig. 7(c). The level of injected mass estimated by these two models is approximately 350 ng for each of the two horizontal features.

IV. LAYERED IMPLOSIONS
A. Frustraum implosion results

In this frustraum campaign, two layered implosions were carried out on the NIF. These layered implosions had a high design adiabat, $\alpha \sim 4.6$, higher than the previous BigFoot platform($\alpha \sim 4$).[3,27–38] This was due to the first shock entering the DT fuel at ~41 km/s and the second shock reaching 72 km/s and merging with the first shock approximately halfway into the ice layer, as opposed to the BigFoot campaign which merged the first and second shocks just before the ice layer and had the combined first and second shocks enter the ice at ~50 km/s. The two frustraum layered implosions were conducted at two different laser energies, which enabled a further test of the effects of coast time on the implosion performance, as has been done previously.[15,39–43] The coast time is defined as the time between the point at which the end of the laser pulse reaches half of its peak power and the time of peak x-ray or gamma ray emission from the hotspot, the bang time of the implosion. The pulse shapes used for the two experiments are shown in Fig. 8 along with the bang times to show the difference in coast times between the two experiments. As listed in Table I, the first layered implosions had a 58.6 μm thick ice layer and the second had a 50.0 μm thick ice layer which also contributed to the change in the coast time. The lower energy implosion, the black pulse shape in Fig. 8, had a coast time of 2.17 ns and the higher energy implosion, the red pulse shape in Fig. 8, had a coast time of 1.75 ns. For the second implosion, the peak power of the laser pulse was also reduced relative to the first layered implosion and that energy placed at the end of the pulse to further extend the pulse length and reduce the coast time. This technique has been used prior to N210725 (Ref. 40) and subsequently on the N210808 shot[5] which was the first shot on the NIF to achieve ignition. These layered implosions had modest backscatter levels from stimulated Brillouin scattering, ~2% for N210117 and ~6% for N210725. Figure 9 shows the time history of the SBS from the 50° cone for the two layered implosions (dashed lines) plotted against the
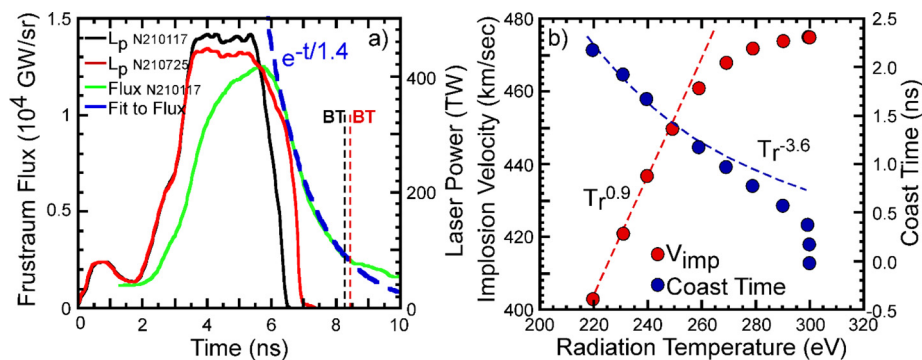
FIG. 8. (a) Laser pulse shapes used for the two layered implosions, N210117 (black) and N210725 (red). The second layered implosion, N210725, used more energy and reduced the peak power, both of which reduced the coast time of the implosion. The flux, measured by the Dante diagnostic, for N210117 (green) along with the analytic (blue) time dependent flux valid once the laser is turned off. (b) Peak implosion velocity (red) and coast time (blue) as a function of the radiation temperature at peak velocity, determined from a Rocket model of N210117 with increasing laser energy.

TABLE I. Summary of target and drive characteristics along with experimentally measured and inferred performance parameters for the frustraum shots and the best performing BigFoot, HDC, and HyE1100 layered implosions.

	Frustraum N210117	Frustraum N210725	HyE1100 N191110	BigFoot N180128	HDC N170827
HDC capsule I.R. (μm)	1200	1200	1100	950	910
W dopant areal density (%μm)	7	7	5.4	6	6.6
Ice layer thickness (μm)	58.6	50	65.5	49.4	55
Laser energy (MJ)	1.6	1.7	1.9	1.8	1.8
Coast time (ns)	2.17	1.76	1.77	0.91	0.53
Neutron image, P0 (μm)	44.9	46	41.9	31	28.4
Neutron image, P2 (μm)	4.5	−20.7	−4.4	0.6	−7.7
Burn width (ps)	209	197	166	152	154
Ion temperature T_{ion} (DT) (keV)	4.26	4.44	4.69	4.88	4.7
Down-scattered ratio DSR (%)	2.44	2.59	3.4	3.09	3.14
DSR/(initial ice thickness) (%/μm)	0.042	0.052	0.052	0.063	0.058
DT neutron yield (13–15 MeV) ($\times 10^{16}$)	1.4	1.9	1.71	1.73	1.66
Yield amplification	1.8	2.2	2.4	2.9	2.9
Capsule absorbed energy E_{cap} (kJ)	234	256	223	166	164
Hotspot energy E_{hs} (kJ)	7.6	9.6	7.8	5	4.5
Hotspot pressure P_{hs} (Gbar)	132	140	168	271	301
GLC $(P_{hs}/420)$sqrt$(E_{hs}/30)$	0.16	0.19	0.2	0.26	0.28

laser pulse shapes (solid line). Further application of four color (using different wavelengths on the two outer cones) is believed to be an avenue for decreasing the SBS on the 50 cone and reducing the overall level of SBS.

A summary of the shot performance is given in Table I for both frustraum shots, as well as the best performing shots in the BigFoot, HDC, and HyE1100 campaigns. The 3D reconstructed hotspot neutron images for the two frustraum layered implosions are seen at the bottom of Fig. 10. The first implosion was nearly round with a P0 of 45 μm and a P2 of 4.5 μm. The second implosion was oblate with a P0

of 46 μm and a P2 of −21 μm. Above and to the left of each of the two reconstructed neutron hotspot images in Fig. 10 are the fluence compensated hotspot images. Looking at all the shots listed in Table I, we see a monotonic increase in hotspot size, P0, capsule absorbed energy, burn width, and hotspot energy with initial capsule diameter. Likewise, as the initial capsule radius increases, we see a decrease in the hotspot pressure, yield amplification, and ion temperature across most of the campaigns. Post-shot integrated *hohlraum* simulations predicted a yield ∼3.5× higher than measured in the experiments.[21]

B. *Hohlraum* cooling and coast time

To isolate the effects of coast time on implosion compression and performance, it has been recognized that this is tied to the *hohlraum* cooling time after the laser is off.[15,39–43] With a few simplifying assumptions, we can calculate the time dependence of the *hohlraum* radiation temperature once the laser is turned off.[44] The energy stored in the *hohlraum* wall during the time that the laser is at peak power can be approximated as $E_{wall} \cong \sigma T_r^4(t') A_{wall}(1 - a_{wall})t_p$ where t_p is the time duration over which the laser is at peak power. To approximate the time dependence of the *hohlraum* radiation temperature, once the laser is turned off, we can set the change in energy stored in the wall over a time Δt, $\left(T_r^4(t' + \Delta t) - T_r^4(t')\right)\sigma A_{wall}(1 - a_{wall})t_p$, equal to the energy lost to radiation exiting the LEHs and absorbed by the capsule, $\sigma T_r^4(t)\left(A_{leh} + A_{cap}(1 - a_{cap})\right)\Delta t$, and the energy lost to heating deeper into wall, $\sigma T_r^4(t)A_{wall}(1 - a_{wall})\Delta t$, such that

$$\frac{1}{T_r^4(t)}\frac{dT_r^4(t)}{dt} = -\frac{A_{leh} + A_{cap}(1 - a_{cap}) + A_{wall}(1 - a_{wall})}{A_{wall}(1 - a_{wall})t_p}, \quad (4)$$

where T_r is the radiation temperature of the cavity, A_{leh} is the total area of both laser entrance holes, A_{cap} and α_{cap} are the area and albedo
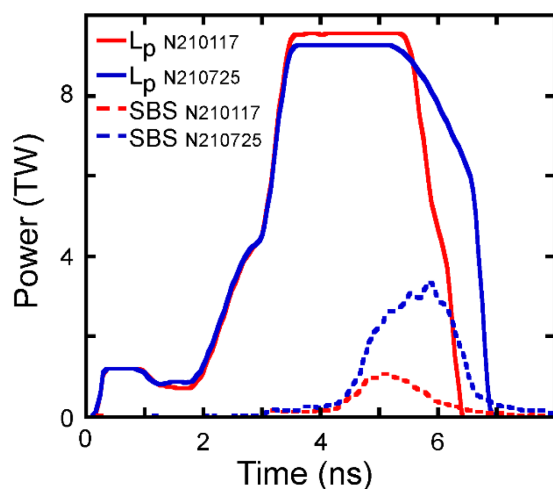
FIG. 9. Plot of the laser power (solid lines) and SBS (dashed lines) for N210117 (red) and N210725 (blue).
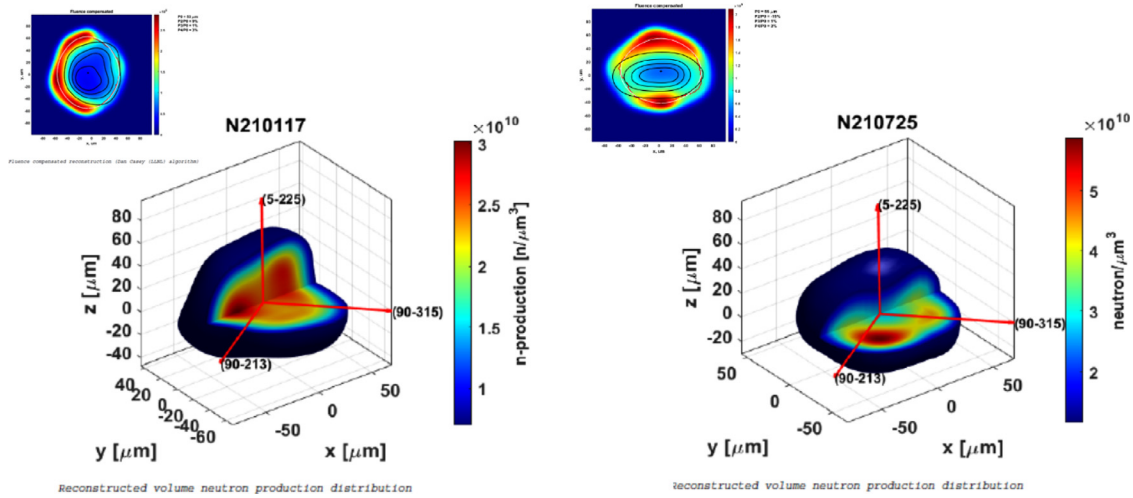
FIG. 10. Reconstructed 3D neutron hotspot shapes for the two layered implosions conducted in the frustraum. The upper left displays the fluence compensated images.

of the capsule after the laser is turned off, and A_{wall} and α_{wall} are the area and flux weighted time-averaged albedo of the wall during peak power. If we ignore the time dependence after the laser is turned off in each of the terms on the right-hand side of the equation, then the solution is simply

$$T_r^4(t) = T_r^4(t_p)e^{\frac{-(A_{leh}+A_{cap}(1-a_{cap})+A_{wall}(1-a_{wall}))t}{A_{wall}(1-a_{wall})t_0}} = T_r^4(t_p)e^{\frac{-t}{t_{cool}}}, \quad (5)$$

where

$$t_{cool} = \frac{A_{wall}(1-a_{wall})t_p}{A_{leh}+A_{cap}(1-a_{cap})+A_{wall}(1-a_{wall})}$$
$$\approx \frac{t_p}{1+A_{leh}/A_{wall}(1-a_{wall})}$$

and the last expression recognizes that the capsule area has greatly shrunk by the time the laser drive is off. One can derive the average albedo of the wall, α_{wall}, for the usual case of a constant peak power pulse for which T_r rises as $t^{0.115}$.[45] The time average of the wall loss,

$T_r^4(1-\alpha_{wall})$, gives a $\alpha_{wall} = 1 - 0.66/(T_r^{0.7}t_p^{0.38})$ for Au, $\alpha_{wall} = 0.83$ for N210117, with T_r at the end of the laser drive in hectoelectron volts and t_p in ns.[45] A more complete analysis leads to a slightly higher albedo, $\alpha_{wall} = 0.89$, as the foot heats the *hohlraum* so that the albedo at the start of peak power is already significant.[46–48] For the higher albedo unlined or Au-lined DU based hohlraums[49] used for most of the DT shots, the 0.66 factor reduces to 0.5 and 0.55, respectively, at $T_r = 3$ heV. So, for example, for the Au-lined DU frustraum shot N210117 with peak $T_r = 2.9$ heV, $t_p = 2$ ns and $(A_{leh} + A_{cap}(1 - \alpha_{cap}))/A_{wall} = .05$, $\alpha_{wall} = 0.89$, and $t_{cool} = 1.4$ ns. This analytic estimate of the time dependent flux (blue) agrees very well with the measured flux for N210117 (green) shown in Fig. 8(a).

C. Stagnated areal density

The effect of the coast time on the down-scattered ratio (DSR)/ (μm of ice) is shown in Figs. 11(a) and 11(b). This includes all of the campaigns on the NIF that used HDC ablators: BigFoot,[3,27–38] HDC,[50–55] Iraum,[56,57] HyB,[4,58] HyE 1100 (Refs. 59 and 60) and HyE
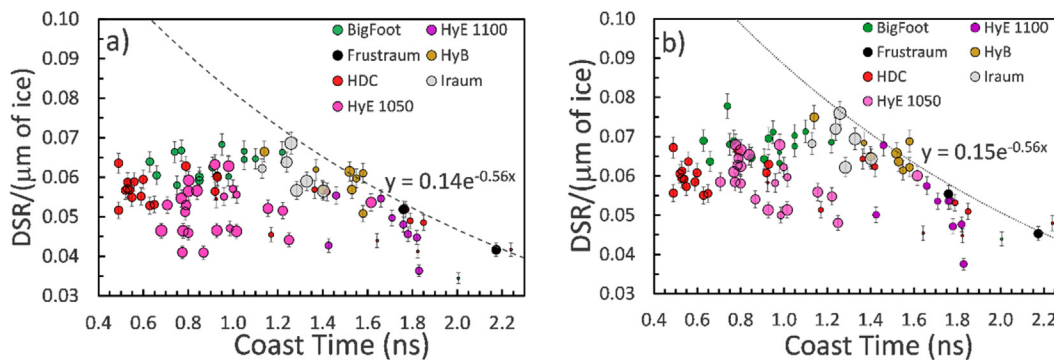
FIG. 11. (a) Down-scattered ratio divided by the initial ice thickness as a function of coast time. (b) Down-scattered ratio divided by the initial ice thickness as a function of coast time corrected for yield amplification, mode 1 and mode 2. The bubble size depends on the tungsten areal density present in each of the capsules used in the implosions.

1050 (Refs. 5, 61, and 62) campaigns, as well as the frustraum shots represented by the black points. The bubble size reflects the dopant areal density $\rho\Delta R$ in units of $\%\mu m$ present in the capsules, where bubble size $= 1000(\rho\Delta R)^2 + 0.5$. In Fig. 11(b), the DSR values have been slightly corrected based on fits to simulations for yield amplification as detailed in Appendix A, $DSR_{cor} = DSR_{meas}/(0.45/(1 + (Y_{amp}/13.7)^{1.56}) + 0.55)$, for P2 mode correction and for P1[63] mode correction, $DSR_{cor} = DSR_{meas}/(1 - DSR_{M1}^2)$. The reduction in DSR with increasing yield amplification is due to the fact that the fuel expands as it burns and a mode 1 asymmetry in the implosion leads to a spatially varying areal density which reduces the overall areal density and DSR of the implosion. The P2 correction assumes DSR for a given fuel mass and volume scales as volume$^{2/3}$/(surface area) approximating surface area-to-volume ratios using oblate and prolate spheroids, which fit DSR vs down-scattered NI P2/P0 in simulations. A larger surface area for a given volume results in a reduction in the areal density and hence in the DSR. As shown in Appendix B, this can be fit by the expression $DSR_{cor} = DSR_{meas}/(1+\chi^*(3^*(P2/P0)/(4+(P2/P0)))^2)$, where the value of $\chi = 0.69$ is used for prolate implosions and increases to $\chi = 0.84$ for oblate implosions. Plotted in this fashion, it is clear that all of the HDC campaigns to date, with coast times >1 ns, are limited in their maximum achievable DSR by their coast time. Figure 11 also shows that the maximum DSR/(μm of ice) and hence effective minimum stagnation adiabat of HDC-based implosions are similar for a given coast time across all campaigns as noted previously.[64] So it is fair to fit the envelope of all campaigns as one universal curve vs coast time, ignoring small variations in t_{cool}. The envelope fit as shown in Fig. 11(a) can be expressed as DSR/(μm of DT ice)$= 0.145\exp(-t_{coast}/1.8) \%/\mu m$.[63] Coast time effects saturate in simulations as the coast time of the implosions becomes smaller than the sum of the sound crossing time in the capsule and the deceleration time of the implosion, ~1 ns.[65] This is apparent in Fig. 10 where we can see that the BigFoot campaign, for instance, has an approximately constant peak DSR/(μm of ice) for coast times less than ~1.2 ns.

To relate t_{cool} to the effects of t_{coast}, an analytic model[63] was developed to relate the stagnated fuel areal density that is inferred from the neutron down-scattered ratio (DSR) to t_{coast}. We can derive a simplified version of this relationship. For adiabatic deceleration of the shell, we have the following expression:

$$P_s R_{hs}^5 = \alpha_{hs} M_{hs}^{5/3}, \quad (6)$$

where P_s is the pressure in the DT shell, R_{hs} is the hotspot radius, α_{hs} is the adiabat of the hotspot, and M_{hs} is the mass of the hotspot. We assume a pressure equilibrium between the shell and the hotspot, P_{hs}, at stagnation such that $P_s \sim P_{hs}$. The outer DT shell radius at stagnation, R_s, is assumed to be proportional to the hotspot radius, $R_s = (fd_i/R_i)^{1/5}R_{hs}$. The parameter f represents the puffing up of fuel due to for example ablator fuel mix preheat. The d_i/R_i term is the initial DT ice thickness to radius ratio, verified by 1D simulations varying d_i for fixed adiabat and implosion velocity. We assume an energy balance between the material inside the outer radius of the shell at stagnation, $P_s R_s^3$, and the peak kinetic energy in the fuel, $M_f V_{imp}^2$

$$P_s R_s^3 \propto M_f v_{imp}^2, \quad (7)$$

where M_f is the initial mass of the DT fuel shell and v_{imp} is the peak implosion velocity. We can substitute Eq. (7) into Eq. (6) and arrive at the following expression:

$$\frac{R_i^2}{R_s^2}\frac{1}{d_i} = \frac{v_{imp}^2}{\alpha_{hs}M_{hs}^{5/3}}\frac{\rho_i R_i^5}{fd_i}, \quad (8)$$

where ρ_i is the initial density of the ice layer, 0.25 g/cm^3. Using mass conservation, we can equate the initial mass in the DT shell, $M_f = 4\pi\rho_i R_i^2 d_i$ and the vapor $(4/3)\pi\rho_g R_i^3$ with the mass in the shell at stagnation, $4_p\rho_s R_s^2 d_s$, and the mass in the hotspot, $(4/3)\pi\rho_{hs}R_{hs}^3$. The down-scattered ratio, DSR, is proportional to the areal density of the DT and hence

$$\frac{DSR}{d_i} \sim \left(\frac{R_i}{R_s}\right)^2\left(\rho_i + \frac{\rho_g R_i}{3d_i}\right) \sim \left(\frac{R_i}{R_s}\right)^2\rho_i. \quad (9)$$

Inserting Eq. (9) into Eq. (8) then allows us to relate the DSR to the peak implosion velocity, the hotspot adiabat, and the hotspot mass[34,35]

$$\frac{DSR}{d_i} \sim \frac{v_{imp}^2}{\alpha_{hs}M_{hs}^{5/3}}\frac{\rho_i^2 R_i^5}{f} \sim \frac{v_{imp}^2}{\alpha_{hs}f}, \quad (10)$$

where the final expression assumes that the vapor mass inside the shell, $(4/3)\pi\rho_g R_i^3$, has been augmented by a fixed fraction by ablation of the inside DT shell, so $M_{hs}^{5/3}$ just scales as R_i^5.

In Ref. 63, the authors used a Rocket model to relate the peak implosion velocity to the *hohlraum*'s radiation temperature at peak velocity. We have taken this same approach to model N210117 and variations of N210117 which change the time duration that the laser was at peak power in order to vary the coast time of the implosion and the radiation temperature at peak implosion velocity, T_{rpv}. The results of this series of rocket model simulations are shown in Fig. 8(b), which shows the coast time and peak implosion velocity as a function of T_{rpv}. For the coast times relevant to the current two frustraum shots, ~1.2–2.2 ns, the peak implosion velocity as a function of the radiation temperature at peak velocity can be fit to a power law, $v_{imp} \sim T_{rpv}^{0.9}$. As such the DSR can be expressed as DSR $\sim (v_{imp}^2/\alpha_s) = (T_r^{1.8}/\alpha_s)$ or with the $t_{cool} = 1.4$ ns for N210117 DSR $\sim (T_r(0)^{1.8}/\alpha_s)\exp(-1.8t/4t_{cool})$. This agrees reasonably well with the empirical fit to the NIF data shown in Fig. 11(a) given in the preceding paragraph.

D. Hotspot performance

The large inner radius of the frustraum capsules, 1200 μm, allows them to absorb large amounts of energy, >250 kJ for N210725, even with the relatively low laser energy of 1.74 MJ. The capsule absorbed energies for the different implosions are seen in Fig. 12, where the bubble size for this plot is proportional to the yield amplification of the implosion and again the two frustraum implosions are represented by the black circles. From this figure, we can see that even though the capsule absorbed energy is higher, the yield amplification remains fairly low, ~2, at these large coast times, similar to the HyE1100 (Refs. 59 and 60) campaign results.

Figure 13(a) shows the primary yield achieved for each of the HDC layered implosions as a function of coast time. Figure 13(b) normalizes the yield by the inner capsule radius to the 4.5 power and the coast time by the capsule inner radius. The bubble size for this plot is proportional to the capsule inner radius, bubble size $= (R_{cap})^5$, of the implosion and again the two frustraum implosions are represented by the black circles and represent the largest two capsules used for indirect-drive layered implosions on the NIF. The larger capsule radius
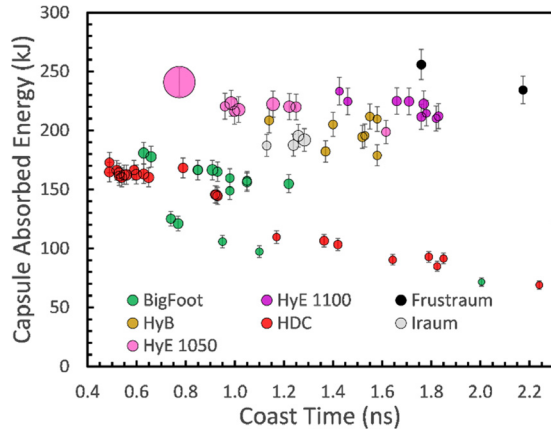
FIG. 12. Bubble plot of capsule absorbed energy vs coast time for all of the HDC campaigns conducted on the NIF. The bubble size depends on the yield amplification for each of the implosions.

and the large *hohlraum* size, however, contributes to the higher coast times for these implosions. The yield for the two frustraum layered implosions is similar to the maximum yield obtained in other HDC campaigns, such as the BigFoot,[3,28–38] HDC[50–55] and Hy1100 (Refs. 59 and 60) campaigns, which all had a maximum yield of $\sim 2 \times 10^{16}$ neutrons. Correcting the shape of the N210725 layered implosion could increase the yield to perhaps 3×10^{16}. The implosions using 1200 μm I.R. capsules in the frustraum campaign, like the implosions using 1100 μm I.R. capsules used in the HyE campaign tended to have higher hotspot energies and lower pressures and yield amplifications than seen in the HDC (910 μm I.R. capsules) and BigFoot (950 μm I.R. capsules) campaigns even though they all achieved similar yields.

As reported in Ref. 30, the ignition threshold factor can be used to formulate a generalized Lawson criteria, GLC, for ignition which includes alpha heating and uses only the directly measured quantities of DSR, primary neutron yield, Y_{13-15}, and the initial ice mass, M_{fuel}. In Ref. 30, this GLC was defined as GLC(ITFXmod) $= 0.27$(ITFXmod)$^{0.6}$, with ITFXmod $\sim$ $(19.7*\text{DSR})^{2}*(0.24*(4f_D f_T)$ $*Y_{13-15}/(M_{fuel}))$. Figure 14(a) shows GLC(ITFXmod) plotted against GLC $= (P_{stag}/420)(E_{hs}/30)^{0.5}$. With GLC(ITFXmod) used in conjunction with the empirical fit of the maximum DSR vs time seen in Fig. 10(a), the minimum yield as a function of coast time can be defined

based on these quantities. The dashed line in Fig. 13 shows this minimum yield required for ignition as a function of coast time. It should be noted that all implosions with coast times less than ~ 1 ns and many shots with coast times >1ns have DSRs lower than the demarcation line. For these implosions the yields required to satisfy GLC(ITFXmod) are higher than the dashed line in Fig. 13. The dashed line in Fig. 13 could, therefore, be thought of as a necessary but not sufficient condition for ignition. A GLC with T_{ion} and DSR can also be formulated from GLC(ITFXmod) in Fig. 14(a) by substituting the yield dependence on DSR and temperature, similar to Eq. (39) of Ref. 66, $Y \propto (M_{fuel})$ DSR$^{0.583}$(T_{ion})$^{5.83}$, into ITFXmod or GLC(DSR, T_{ion}) $= (0.187)$DSR$^{1.55}$Tion$^{3.5}$ as shown in Fig. 14(b). There is more uncertainty in this definition of GLC than in the GLC(ITFXmod), but it allows us to use the demarcation line in DSR along with GLC(DSR, T_{ion}) to determine a minimum T_{ion} vs coast time for ignition which is then plotted in Fig. 15.

Figure 15 shows the ion temperature from all of the HDC layered DT implosions conducted on the NIF. Again, the two frustraum implosions are represented by the black circles. The bubble size reflects the dopant areal density as in Fig. 10. The larger hotspot size, due to the larger initial capsule radius and the long coast time affecting the compression, results in ion temperatures that are slightly lower than in the HyE1100 campaign. The dashed line in Fig. 15 represents the minimum T_{ion} required to reach ignition as a function of coast time. Again, it should be noted that all implosions with coast times less than ~ 1 ns and many implosions with coast times >1 ns have DSRs lower than the demarcation line and so the ion temperatures required to satisfy GLC(DSR, T_{ion}) for those implosions are higher than the dashed line in Fig. 15.

V. SUMMARY

Most efforts to improve performance of layered implosions to date have focused on increasing the capsule size to increase the surface area and the capsule absorbed energy. In this article, we extend this approach by fielding the largest HDC capsules, 1.2 mm inner radius, to date for indirect-drive inertial confinement fusion. Even at 1.74 MJ of laser energy, this surpassed the previous indirect-drive capsule absorbed energies achieved in layered implosions on the NIF at energies less than 2.05 MJ. These larger capsules and frustraum sizes with the limited energy available on the NIF, however, resulted in long coast times, ≥ 1.75 ns. The long coast times reduced the *hohlraum* drive onto the capsule by the time of peak compression and resulted in
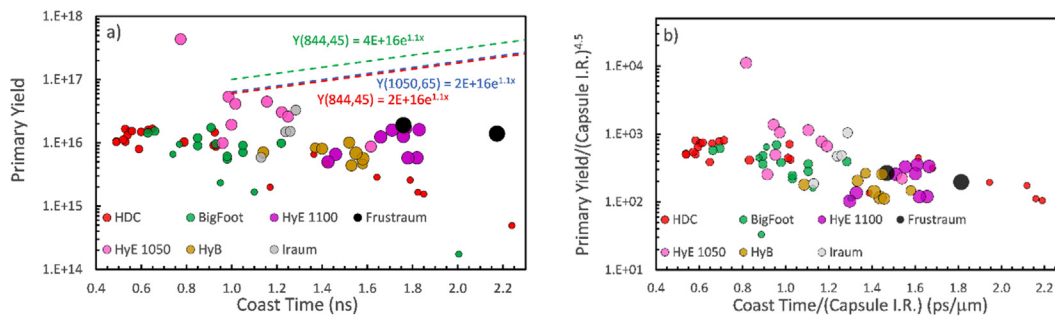
FIG. 13. (a) Bubble plot of primary neutron yield vs coast time for all of the HDC campaigns conducted on the NIF. The bubble size depends on the radius of the capsule to the fifth power for each of the implosions. (b) The y-axis has the yield/(capsule radius)$^{4.5}$ vs the coast time/(capsule radius).
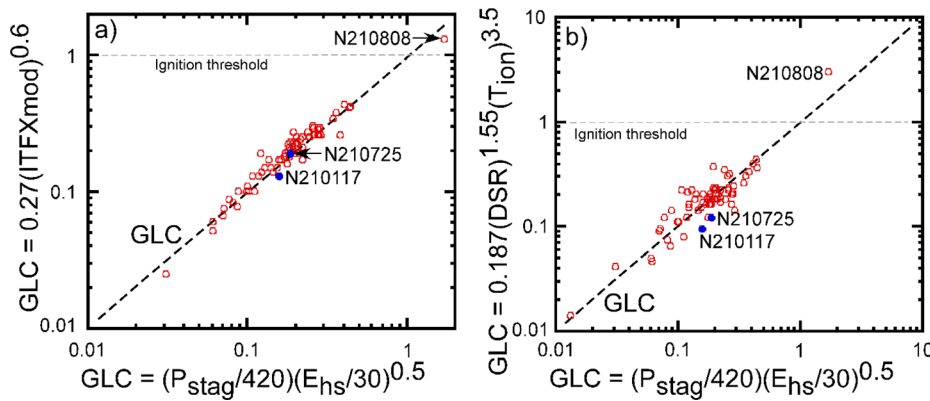
FIG. 14. Generalized Lawson criterion using the $GLC(ITFXmod) = 0.27(ITFXmod)^{0.6}$ plotted against the $GLC(P_{stag}, E_{hs}) = (P_{stag}/420)(E_{hs}/30)^{0.5}$ is shown in (a). Generalized Lawson criterion using the $GLC(DSR, Tion) = 0.187(DSR)^{1.55}(T_{ion})^{3.5}$ plotted against the $GLC(P_{stag}, E_{hs}) = (P_{stag}/420)(E_{hs}/30)^{0.5}$ is shown in (b).

lower DSR values. We presented the results of these implosions along with all of the HDC layered implosions conducted on the NIF. This allowed us to conclude that by looking at the DSR vs coast time results that there is a maximum achievable DSR for all of the HDC campaigns on the NIF, including the frustraum campaign. The maximum DSR/(μm of DT ice) across the different campaigns was found to be expressed as DSR/(μm of DT ice) $= 0.15\exp(-0.56*t_{coast})$ %/μm and for the long coast times in the frustraum layered implosions, both experiments fell close to this line. We previously derived a generalized Lawson criterion based on the ignition threshold factor and used that in conjunction with maximum DSR as a function of coast time to derive a minimum yield required for ignition as a function of coast time. Similarly, we put the yield in terms of DSR and T_{ion} which allowed us to derive minimum ion temperature as a function of coast time for ignition as well. These minima as a function of coast time suggest that increasing the energy absorbed by the capsule at the expense of long coast times makes it more challenging to achieve ignition and

that further reducing coast time closer to the 1 ns level is warranted to improve the areal density and make it easier to achieve the hotspot temperature, alpha heating, and yield amplification required for ignition.

We are in the process of improving the performance of this platform by reducing the overall size of the frustraum by ~15% and the capsule diameter by 9%, 1.1 mm I.R., to enable higher radiation drive and shorter coast times, ~1 ns. In addition, the laser pulse shape is adjusted to reduce the design adiabat of the implosions from >4 in the current platform to <3 to increase the DSR of the implosions. We have also moved the 44.5° cone closer to the capsule and the 50° cone further away, relative to the 44.5° cone, to reduce the level of P4 seen in the current platform and we will report on this work in a later article.

ACKNOWLEDGMENTS

AUTHOR DECLARATIONS
Conflict of Interest

The authors have no conflicts to disclose.

Author Contributions

Kevin Baker: Data curation (equal); Formal analysis (equal); Investigation (equal); Methodology (equal); Writing – original draft (equal); Writing – review & editing (equal). **Peter Andrew Amendt:** Conceptualization (equal); Formal analysis (equal); Investigation (equal). **James S. Ross:** Data curation (equal); Formal analysis (equal); Investigation (equal); Supervision (equal). **V. A. Smalyuk:** Project administration (equal); Supervision (equal). **Otto L. Landen:** Formal analysis (equal); Methodology (equal); Supervision (equal); Writing – review & editing (equal). **Darwin D.-M. Ho:** Formal analysis (equal); Investigation (equal). **Shahab Firasat Khan:** Formal analysis (equal). **Steven W. Haan:** Formal analysis (equal). **John Lindl:** Formal analysis (equal); Supervision (equal); Writing – review & editing (equal).
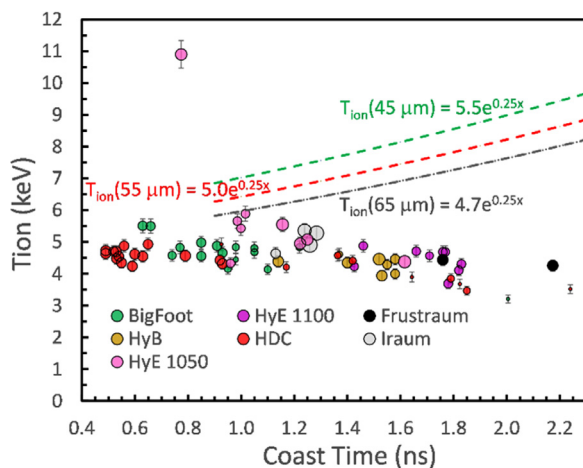
FIG. 15. Bubble plot of the ion temperature vs coast time for all of the HDC campaigns conducted on the NIF. The dashed line represents the minimum ion temperature vs coast time required for ignition using the GLC defined in (b) along with the DSR represented by the dashed line in Fig. 12. The bubble size depends on the radius of the capsule to the fifth power for each of the implosions. All experiments with coast time less than 1 ns have DSRs lower than the dashed line in Fig. 12 and hence would require a higher T_{ion} for ignition than the minimum T_{ion} line.

Derek Alexander Mariscal: Data curation (equal). **Jose L. Milovich:** Investigation (equal). **Stephan A. MacLaren:** Formal analysis (equal). **Yuan Ping:** Data curation (equal). **David J. Strozzi:** Formal analysis (equal); Writing – review & editing (equal). **Richard Marshall Bionta:** Formal analysis (equal). **Daniel T. Casey:** Formal analysis (equal). **Peter M. Celliers:** Formal analysis (equal). **David N. Fittinghoff:** Formal analysis (equal). **Hermann Geppert-Kleinrath:** Formal analysis (equal). **Verena Geppert-Kleinrath:** Formal analysis (equal). **Kelly Hahn:** Formal analysis (equal). **Maria Gatu Johnson:** Formal analysis (equal). **Yongho Kim:** Formal analysis (equal). **Kevin Meaney:** Formal analysis (equal). **Marius Millot:** Formal analysis (equal); Writing – review & editing (equal). **Ryan Charles Nora:** Formal analysis (equal). **Petr Volegov:** Formal analysis (equal). **Carl Wilde:** Formal analysis (equal).

DATA AVAILABILITY

The data that support the findings of this study are available from the corresponding author upon reasonable request.

APPENDIX A: CORRECTION OF THE DOWN-SCATTERED RATIO (DSR) DUE TO YIELD AMPLIFICATION

Simulations show that as the DT fuel burns it expands and this expansion causes a reduction in the measured DSR.[66] In Fig. 41(c) of Ref. 66, the authors plotted the ratio of the DSR with alpha heating, DSR_α, to the DSR without alpha heating, $DSR_{no-\alpha}$, as a function of yield amplification to illustrate this effect. Figure 16(a) includes a larger number of simulations and a fit to these data shows that we can express the reduction in DSR with yield amplification as

$$\frac{DSR_\alpha}{DSR_{no-\alpha}} = 0.55 + \frac{0.45}{1 + \left(\frac{Y_{amp}}{13.7}\right)^{1.56}}. \qquad (A1)$$

We have also made modifications to our previous definition of yield amplification with alpha heating[30] to account for the behavior at large levels of yield amplification. Figure 16(b) shows the simulated yield amplification as a function of the experimentally observable ignition threshold factor ($ITFX_{mod}$). In Fig. 16(b), the maximum yield amplification depends on the areal density of the design.[66] We keep the definition of $ITFX_{mod}$ in Ref. 30 as

$$ITFX_{mod} = \frac{(19.7DSR)^2 (0.24(4f_D f_T)Y_{13-15})}{M_{fuel}}, \qquad (A2)$$

where DSR is the down scattered ratio (the ratio of the neutron yield in the neutron kinetic energy range from 10–12 MeV to the 13–15 MeV range), f_D is the deuterium number fraction in the hotspot, f_T is the tritium number fraction in the hotspot, Y_{13-15} is the primary neutron yield/10^{16}, and M_{fuel} is the initial mass of the ice layer in mg. We can then fit the simulated data in Fig. 16(b) with the following expression:

$$Y_{amp-ITFXmod} = \exp\left(0.85\left(\frac{ITFX_{mod}}{1 + 0.009(ITFX_{mod})}\right)^{0.46}\right), \qquad (A3)$$
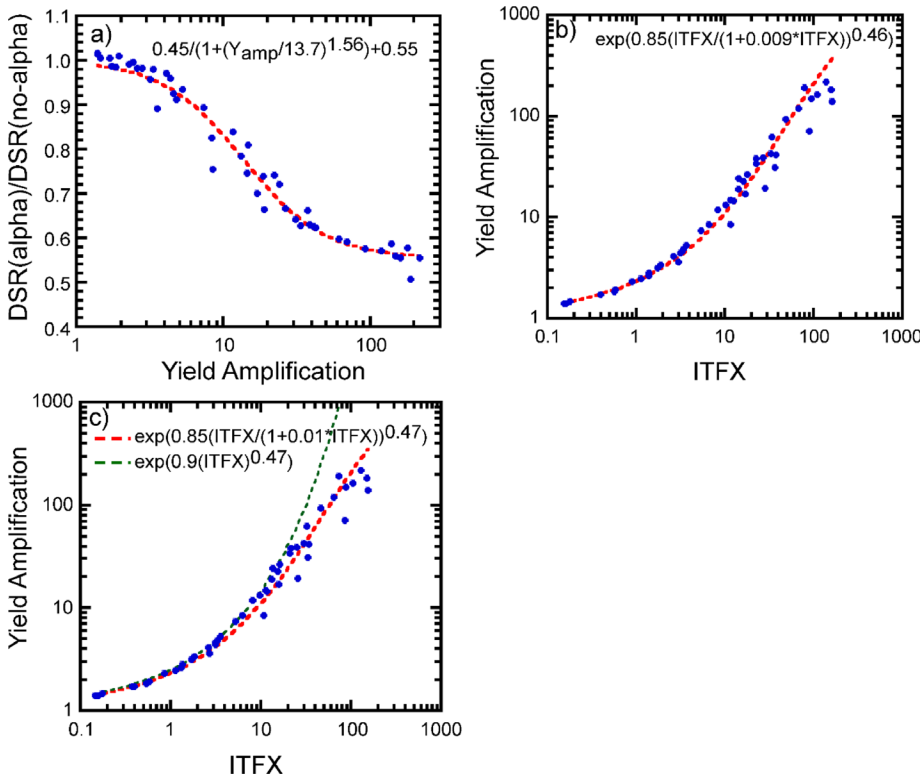
FIG. 16. (a) Ratio of the DSR with alpha heating to the DSR without alpha heating as a function of yield amplification. (b) Yield amplification as a function of ITFXmod. (c) Yield amplification as a function of ITFX.

which is the definition for yield amplification used in this article. We can also use the definition of ITFX in Ref. 32 to define an expression for yield amplification that better fits implosions with large yield amplification. In Ref. 32, ITFX with alpha heating is defined as

$$ITFX = \left(\frac{170}{M_{fuel}}\right)\left(\frac{Y_{13-15}}{4 \times 10^{15}}\right)\left(\frac{DSR}{0.067}\right)^{2.1}, \qquad (A4)$$

where DSR is the measured down scattered ratio (the ratio of the neutron yield in the neutron kinetic energy range from 10–12 MeV to the 13–15 MeV range), Y_{13-15} is the primary neutron yield, and M_{fuel} is the initial mass of the ice layer in μg. We can then fit the simulated data in Fig. 16(c) with the following expression:

$$Y_{amp} = \exp\left(0.85\left(\frac{ITFX}{1 + 0.01(ITFX)}\right)^{0.47}\right) \qquad (A5)$$

to better fit implosions across all yield amplification levels.

APPENDIX B: MODE 2 CORRECTION FOR THE DOWN-SCATTERED RATIO (DSR)

The mode P2 degradation of the DSR for a given fuel mass and volume scales as volume$^{2/3}$/(surface area). One can numerically solve for the surface area of the spherical harmonics[67] used to describe the hotspot or approximate the surface area-to-volume ratios analytically using oblate and prolate spheroids and then relate the Legendre polynomials to the equatorial and polar radius of the spheroid as done below. For a spheroid with the z axis representing the symmetry axis, the cartesian equation describing the surface is given as

$$\frac{x^2 + y^2}{a^2} + \frac{z^2}{c^2} = 1. \qquad (B1)$$

For a prolate ellipsoid, c > a, the surface area is given by

$$2\pi a^2 \left(1 + \frac{\left(\frac{c}{a}\right)^2}{\sqrt{\left(\frac{c}{a}\right)^2 - 1}} \sin^{-1}\sqrt{1 - \left(\frac{a}{c}\right)^2}\right) \qquad (B2)$$

and for an oblate ellipsoid, a > c, the surface area is

$$2\pi a^2 \left(1 + \frac{\left(\frac{c}{a}\right)^2}{\sqrt{1 - \left(\frac{c}{a}\right)^2}} ln\left(\frac{1 + \sqrt{1 - \left(\frac{c}{a}\right)^2}}{1 - \sqrt{1 - \left(\frac{c}{a}\right)^2}}\right)\right). \qquad (B3)$$

The volume of an ellipsod is expressed as

$$\frac{4}{3}\pi a^2 c. \qquad (B4)$$

The radii of the ellipsoid are related to the Legendre modes P2/P0 through the following relation:[68]
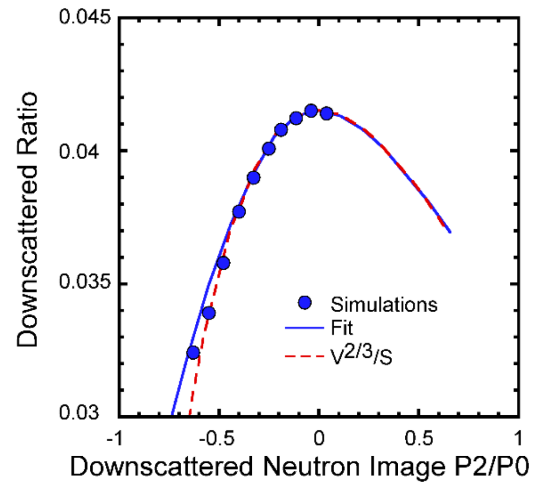
FIG. 17. Plot of the simulated DSR degradation, black circles, due to mode 2 shape. The dashed red line denotes an analytic fit of V$^{2/3}$/S to the DSR as a function of P2/P0, where V is the volume of a spheroid, S is the surface area of the spheroid, P2 is the mode 2 of the fuel, and P0 is the fuel radius.

$$\frac{c}{a} = \frac{1 + \frac{P2}{P0}}{1 - 0.5\left(\frac{P2}{P0}\right)}. \qquad (B5)$$

We can then compare the analytic expression of the DSR degradation, volume$^{2/3}$/(surface area), dashed red line, to the downscattered DSR vs NI P2/P0 seen in simulations, black circles, as shown in Fig. 17. We can also fit a simplified expression to the simulations and the volume$^{2/3}$/(surface area), which is what we use in the paper to correct the DSR to mode 2. This fit, blue line, is shown in Fig. 17 and is expressed as $(1+\chi^*(3^*(P2/P0)/(4+(P2/P0)))^2)$, where the value of $\chi = 0.69$ is used for prolate implosions and increases to $\chi = 0.84$ for oblate implosions.

REFERENCES

[1]J. Lindl, "Development of the indirect-drive approach to inertial confinement fusion and the target physics basis for ignition and gain," Phys. Plasmas **2**, 3933–4024 (1995).

[2]S. Atzeni and J. Meyer-ter-Vehn, *The Physics of Inertial Fusion* (Oxford University Press, 2008).

[3]K. L. Baker, O. Jones, C. Weber, D. Clark, P. K. Patel, C. A. Thomas, O. L. Landen, R. Nora, G. J. Anderson, J. Gaffney, S. MacLaren, D. T. Casey, T. Döppner, E. L. Dewald, R. Tommasini, B. K. Spears, J. Salmonson, M. Hohenberger, S. Khan, A. Zylstra, A. Kritcher, P. Amendt, V. Smalyuk, J. Lindl, C. Young, J. S. Ross, D. Ho, O. A. Hurricane, D. A. Callahan, T. Woods, J. L. Milovich, D. J. Strozzi, B. Bachmann, R. Bionta, P. M. Celliers, D. Fittinghoff, R. Hatarik, M. Gatu Johnson, K. Meaney, M. Millot, P. L. Volegov, and C. Wilde, "Hydroscaling indirect-drive implosions on the National Ignition Facility," Phys. Plasmas **29**, 062705 (2022).

[4]A. L. Kritcher, D. T. Casey, C. A. Thomas, A. B. Zylstra, M. Hohenberger, K. Baker, S. Le Pape, B. Bachmann, S. Bhandarkar, J. Biener, T. Braun, D. Clark, L. Divol, T. Döppner, D. Hinkel, C. Kong, D. Mariscal, M. Millot, J. Milovich, A. Nikroo, A. Pak, N. Rice, H. Robey, M. Stadermann, J. Sevier, D. Strozzi, C. Weber, C. Wild, B. Woodworth, J. Edwards, D. A. Callahan, and O. A. Hurricane, "Symmetric fielding of the largest diamond capsule implosions on the NIF," Phys. Plasmas **27**, 052710 (2020).

[5]H. Abu-Shawareb, R. Acree, P. Adams, J. Adams, B. Addis, R. Aden, P. Adrian, B. B. Afeyan, M. Aggleton, L. Aghaian, A. Aguirre, D. Aikens, J. Akre, F. Albert, M. Albrecht, B. J. Albright, J. Albritton, J. Alcala, C. Alday, D. A. Alessi, N. Alexander, J. Alfonso, N. Alfonso, E. Alger, S. J. Ali, Z. A. Ali, W. E. Alley, P. Amala, P. A. Amendt, P. Amick, S. Ammula, C. Amorin, D. J. Ampleford, R. W. Anderson, T. Anklam, N. Antipa, B. Appelbe, C. Aracne-Ruddle, E. Araya, M. Arend, P. Arnold, T. Arnold, J. Asay, L. J. Atherton, D. Atkinson, R. Atkinson, J. M. Auerbach, B. Austin, L. Auyang, A. S. Awwal, J. Ayers, S. Ayers, T. Ayers, S. Azevedo, B. Bachmann, C. A. Back, J. Bae, D. S. Bailey, J. Bailey, T. Baisden, K. L. Baker, H. Baldis, D. Barber, M. Barberis, D. Barker, A. Barnes, C. W. Barnes, M. A. Barrios, C. Barty, I. Bass, S. H. Batha, S. H. Baxamusa, G. Bazan, J. K. Beagle, R. Beale, B. R. Beck, J. B. Beck, M. Bedzyk, R. G. Beeler, R. G. Beeler, W. Behrendt, L. Belk, P. Bell, M. Belyaev, J. F. Benage, G. Bennett, L. R. Benedetti, L. X. Benedict, R. Berger, T. Bernat, L. A. Bernstein, B. Berry, L. Bertolini, G. Besenbruch, J. Betcher, R. Bettenhausen, R. Betti, B. Bezzerides, S. D. Bhandarkar, R. Bickel, J. Biener, T. Biesiada, K. Bigelow, J. Bigelow-Granillo, V. Bigman, R. M. Bionta, N. W. Birge, M. Bitter, A. C. Black, R. Bleile, D. L. Bleuel, E. Bliss, E. Bliss, B. Blue, T. Boehly, K. Boehm, C. D. Boley, R. Bonanno, E. J. Bond, T. Bond, M. J. Bonino, M. Borden, J. L. Bourgade, J. Bousquet, J. Bowers, M. Bowers, R. Boyd, A. Bozek, D. K. Bradley, K. S. Bradley, P. A. Bradley, L. Bradley, L. Brannon, P. S. Brantley, D. Braun, T. Braun, K. Brienza-Larsen, T. M. Briggs, J. Britten, E. D. Brooks, D. Browning, M. W. Bruhn, T. A. Brunner, H. Bruns, G. Brunton, B. Bryant, T. Buczek, J. Bude, L. Buitano, S. Burkhart, J. Burmark, A. Burnham, R. Burr, L. E. Busby, B. Butlin, R. Cabeltis, M. Cable, W. H. Cabot, B. Cagadas, J. Caggiano, R. Cahayag, S. E. Caldwell, S. Calkins, D. A. Callahan, J. Calleja-Aguirre, L. Camara, D. Camp, E. M. Campbell, J. H. Campbell, B. Carey, R. Carey, K. Carlisle, L. Carlson, L. Carman, J. Carmichael, A. Carpenter, C. Carr, J. A. Carrera, D. Casavant, A. Casey, D. T. Casey, A. Castillo, E. Castillo, J. I. Castor, C. Castro, W. Caughey, R. Cavitt, J. Celeste, P. M. Celliers, C. Cerjan, G. Chandler, B. Chang, C. Chang, J. Chang, L. Chang, R. Chapman, T. Chapman, L. Chase, H. Chen, H. Chen, K. Chen, L. Y. Chen, B. Cheng, J. Chittenden, C. Choate, J. Chou, R. E. Chrien, M. Chrisp, K. Christensen, M. Christensen, A. R. Christopherson, M. Chung, J. A. Church, A. Clark, D. S. Clark, K. Clark, R. Clark, L. Claus, B. Cline, J. A. Cline, J. A. Cobble, K. Cochrane, B. Cohen, S. Cohen, M. R. Collette, G. Collins, L. A. Collins, T. J. B. Collins, A. Conder, B. Conrad, M. Conyers, A. W. Cook, D. Cook, R. Cook, J. C. Cooley, G. Cooper, T. Cope, S. R. Copeland, F. Coppari, J. Cortez, J. Cox, D. H. Crandall, J. Crane, R. S. Craxton, M. Cray, A. Crilly, J. W. Crippen, D. Cross, M. Cuneo, G. Cuotts, C. E. Czajka, D. Czechowicz, T. Daly, P. Danforth, R. Darbee, B. Darlington, P. Datte, L. Dauffy, G. Davalos, S. Davidovits, P. Davis, J. Davis, S. Dawson, R. D. Day, T. H. Day, M. Dayton, C. Deck, C. Decker, C. Deeney, K. A. DeFriend, G. Deis, N. D. Delamater, J. A. Delettrez, R. Demaret, S. Demos, S. M. Dempsey, R. Desjardin, T. Desjardins, M. P. Desjarlais, E. L. Dewald, J. DeYoreo, S. Diaz, G. Dimonte, T. R. Dittrich, L. Divol, S. N. Dixit, J. Dixon, E. S. Dodd, D. Dolan, A. Donovan, M. Donovan, T. Doppner, C. Dorrer, N. Dorsano, M. R. Douglas, D. Dow, J. Downie, E. Downing, M. Dozieres, V. Draggoo, D. Drake, R. P. Drake, T. Drake, G. Dreifuerst, D. F. DuBois, P. F. DuBois, G. Dunham, R. Dylla-Spears, A. K. L. Dymoke-Bradshaw, B. Dzenitis, C. Ebbers, M. Eckart, S. Eddinger, D. Eder, D. Edgell, M. J. Edwards, P. Efthimion, J. H. Eggert, B. Ehrlich, P. Ehrmann, S. Elhadj, C. Ellerbee, N. S. Elliott, C. L. Ellison, F. Elsner, M. Emerich, K. Engelhorn, T. England, E. English, P. Epperson, R. Epstein, G. Erbert, M. A. Erickson, D. J. Erskine, A. Erlandson, R. J. Espinosa, C. Estes, K. G. Estabrook, S. Evans, A. Fabyan, J. Fair, R. Fallejo, N. Farmer, W. A. Farmer, M. Farrell, V. E. Fatherley, M. Fedorov, R. Feigenbaum, M. Feit, W. Ferguson, J. C. Fernandez, A. Fernandez-Panella, S. Fess, J. E. Field, C. V. Filip, J. R. Fincke, T. Finn, S. M. Finnegan, R. G. Finucane, M. Fischer, A. Fisher, J. Fisher, B. Fishler, D. Fittinghoff, P. Fitzsimmons, M. Flegel, K. A. Flippo, J. Florio, J. Folta, P. Folta, L. R. Foreman, C. Forrest, A. Forsman, J. Fooks, M. Foord, R. Fortner, K. Fournier, D. E. Fratanduono, N. Frazier, T. Frazier, C. Frederick, M. S. Freeman, J. Frenje, D. Frey, G. Frieders, S. Friedrich, D. H. Froula, J. Fry, T. Fuller, J. Gaffney, S. Gales, B. L. Galloudec, K. K. L. Galloudec, A. Gambhir, L. Gao, W. J. Garbett, A. Garcia, C. Gates, E. Gaut, P. Gauthier, Z. Gavin, J. Gaylord, M. Geissel, F. Genin, J. Georgeson, H. Geppert-Kleinrath, V. Geppert-Kleinrath, N. Gharibyan, J. Gibson, C. Gibson, E. Giraldez, V. Glebov, S. G. Glendinning, S. Glenn, S. H. Glenzer, S. Goade, P. L. Gobby, S. R.

Goldman, B. Golick, M. Gomez, V. Goncharov, D. Goodin, P. Grabowski, E. Grafil, P. Graham, J. Grandy, E. Grasz, F. Graziani, G. Greenman, J. A. Greenough, A. Greenwood, G. Gregori, T. Green, J. R. Griego, G. P. Grim, J. Grondalski, S. Gross, J. Guckian, N. Guler, A. Gunney, G. Guss, S. Haan, J. Hackbarth, L. Hackel, R. Hackel, C. Haefner, C. Hagmann, K. D. Hahn, S. Hahn, B. J. Haid, B. M. Haines, B. M. Hall, C. Hall, G. N. Hall, M. Hamamoto, S. Hamel, C. E. Hamilton, B. A. Hammel, J. H. Hammer, G. Hampton, A. Hamza, A. Handler, S. Hansen, D. Hanson, R. Haque, D. Harding, E. Harding, J. D. Hares, D. B. Harris, J. A. Harte, E. P. Hartouni, R. Hatarik, S. Hatchett, A. A. Hauer, M. Havre, R. Hawley, J. Hayes, J. Hayes, S. Hayes, A. Hayes-Sterbenz, C. A. Haynam, D. A. Haynes, D. Headley, A. Heal, J. E. Heebner, S. Heerey, G. M. Heestand, R. Heeter, N. Hein, C. Heinbockel, C. Hendricks, M. Henesian, J. Heninger, J. Henrikson, E. A. Henry, E. B. Herbold, M. R. Hermann, G. Hermes, J. E. Hernandez, V. J. Hernandez, M. C. Herrmann, H. W. Herrmann, O. D. Herrera, D. Hewett, R. Hibbard, D. G. Hicks, D. Hill, K. Hill, T. Hilsabeck, D. E. Hinkel, D. D. Ho, V. K. Ho, J. K. Hoffer, N. M. Hoffman, M. Hohenberger, M. Hohensee, W. Hoke, D. Holdener, F. Holdener, J. P. Holder, B. Holko, D. Holunga, J. F. Holzrichter, J. Honig, D. Hoover, D. Hopkins, L. Berzak Hopkins, M. Hoppe, M. L. Hoppe, J. Horner, R. Hornung, C. J. Horsfield, J. Horvath, D. Hotaling, R. House, L. Howell, W. W. Hsing, S. X. Hu, H. Huang, J. Huckins, H. Hui, K. D. Humbird, J. Hund, J. Hunt, O. A. Hurricane, M. Hutton, K. H. Huynh, L. Inandan, C. Iglesias, I. V. Igumenshchev, N. Izumi, M. Jackson, J. Jackson, S. D. Jacobs, G. James, K. Jancaitis, J. Jarboe, L. C. Jarrott, D. Jasion, J. Jaquez, J. Jeet, A. E. Jenei, J. Jensen, J. Jimenez, R. Jimenez, D. Jobe, Z. Johal, H. M. Johns, D. Johnson, M. A. Johnson, M. Gatu Johnson, R. J. Johnson, S. Johnson, S. A. Johnson, T. Johnson, K. Jones, O. Jones, M. Jones, S. Jones, R. Jorge, H. J. Jorgenson, M. Julian, B. I. Jun, R. Jungquist, J. Kaae, N. Kabadi, D. Kaczala, D. Kalantar, K. Kangas, V. V. Karasiev, M. Karasik, V. Karpenko, A. Kasarky, K. Kasper, R. Kauffman, M. I. Kaufman, C. Keane, L. Keaty, L. Kegelmeyer, P. A. Keiter, P. A. Kellett, J. Kellogg, J. H. Kelly, S. Kemic, A. J. Kemp, G. E. Kemp, G. D. Kerbel, D. Kershaw, S. M. Kerr, T. J. Kessler, M. H. Key, S. F. Khan, H. Khater, C. Kiikka, J. Kilkenny, Y. Kim, Y. J. Kim, J. Kimko, M. Kimmel, J. M. Kindel, J. King, R. K. Kirkwood, L. Klaus, D. Klem, J. L. Kline, J. Klingmann, G. Kluth, P. Knapp, J. Knauer, J. Knipping, M. Knudson, D. Kobs, J. Koch, T. Kohut, C. Kong, J. M. Koning, P. Koning, S. Konior, H. Kornblum, L. B. Kot, B. Kozioziemski, M. Kozlowski, P. M. Kozlowski, J. Krammen, N. S. Krasheninnikova, B. Kraus, W. Krauser, J. D. Kress, A. L. Kritcher, E. Krieger, J. J. Kroll, W. L. Kruer, M. K. G. Kruse, S. Kucheyev, M. Kumbera, S. Kumpan, J. Kunimune, B. Kustowski, T. J. T. Kwan, G. A. Kyrala, S. Laffite, M. Lafon, K. LaFortune, B. Lahmann, B. Lairson, O. L. Landen, J. Langenbrunner, L. Lagin, T. Land, M. Lane, D. Laney, A. B. Langdon, S. H. Langer, A. Langro, N. E. Lanier, T. E. Lanier, D. Larson, B. F. Lasinski, D. Lassle, D. LaTray, G. Lau, N. Lau, C. Laumann, A. Laurence, T. A. Laurence, J. Lawson, H. P. Le, R. R. Leach, L. Leal, A. Leatherland, K. LeChien, B. Lechleiter, A. Lee, M. Lee, T. Lee, R. J. Leeper, E. Lefebvre, J. P. Leidinger, B. LeMire, R. W. Lemke, N. C. Lemos, S. L. Pape, R. Lerche, S. Lerner, S. Letts, K. Levedahl, T. Lewis, C. K. Li, H. Li, J. Li, W. Liao, Z. M. Liao, D. Liedahl, J. Liebman, G. Lindford, E. L. Lindman, J. D. Lindl, H. Loey, R. A. London, F. Long, E. N. Loomis, E. Lopez, H. Lopez, E. Losbanos, S. Loucks, R. Lowe-Webb, E. Lundgren, A. P. Ludwigsen, R. Luo, J. Lusk, R. Lyons, T. Ma, Y. Macallop, M. J. MacDonald, B. J. MacGowan, J. M. Mack, A. J. Mackinnon, S. A. MacLaren, A. G. MacPhee, G. R. Magelssen, J. Magoon, R. M. Malone, T. Malsbury, R. Managan, R. Mancini, K. Manes, D. Maney, D. Manha, O. M. Mannion, A. M. Manuel, E. Mapoles, G. Mara, T. Marcotte, E. Marin, M. M. Marinak, C. Mariscal, D. A. Mariscal, E. F. Mariscal, E. V. Marley, J. A. Marozas, S. Marquez, C. D. Marshall, F. J. Marshall, M. Marshall, S. Marshall, J. Marticorena, D. Martinez, I. Maslennikov, D. Mason, R. J. Mason, L. Masse, W. Massey, P. E. Masson-Laborde, N. D. Masters, D. Mathisen, E. Mathison, J. Matone, M. J. Matthews, C. Mattoon, T. R. Mattsson, K. Matzen, C. W. Mauche, M. Mauldin, T. McAbee, M. McBurney, T. McCarville, R. L. McCrory, A. M. McEvoy, C. McGuffey, M. McInnis, P. McKenty, M. S. McKinley, J. B. McLeod, A. McPherson, B. McQuillan, M. Meamber, K. D. Meaney, N. B. Meezan, R. Meissner, T. A. Mehlhorn, N. C. Mehta, J. Menapace, F. E. Merrill, B. T. Merritt, E. C. Merritt, D. D. Meyerhofer, S. Mezyk, R. J. Mich, P. A. Michel, D. Milam, C. Miller, D. Miller, D. S. Miller, E. Miller, E. K. Miller, J. Miller, M. Miller, P. E. Miller, T. Miller, W. Miller, V. Miller-Kamm, M. Millot, J. L. Milovich, P. Minner, J. L. Miquel,

S. Mitchell, K. Molvig, R. C. Montesanti, D. S. Montgomery, M. Monticelli, A. Montoya, J. D. Moody, A. S. Moore, E. Moore, M. Moran, J. C. Moreno, K. Moreno, B. E. Morgan, T. Morrow, J. W. Morton, E. Moses, K. Moy, R. Muir, M. S. Murillo, J. E. Murray, J. R. Murray, D. H. Munro, T. J. Murphy, F. M. Munteanu, J. Nafziger, T. Nagayama, S. R. Nagel, R. Nast, R. A. Negres, A. Nelson, D. Nelson, J. Nelson, S. Nelson, S. Nemethy, P. Neumayer, K. Newman, M. Newton, H. Nguyen, J. G. Di Nicola, P. Di Nicola, C. Niemann, A. Nikroo, P. M. Nilson, A. Nobile, V. Noorai, R. Nora, M. Norton, M. Nostrand, V. Note, S. Novell, P. F. Nowak, A. Nunez, R. A. Nyholm, M. O'Brien, A. Oceguera, J. A. Oertel, J. Okui, B. Olejniczak, J. Oliveira, P. Olsen, B. Olson, K. Olson, R. E. Olson, Y. P. Opachich, N. Orsi, C. D. Orth, M. Owen, S. Padalino, E. Padilla, R. Paguio, S. Paguio, J. Paisner, S. Pajoom, A. Pak, S. Palaniyappan, K. Palma, T. Pannell, F. Papp, D. Paras, T. Parham, H. S. Park, A. Pasternak, S. Patankar, M. V. Patel, P. K. Patel, R. Patterson, S. Patterson, B. Paul, M. Paul, E. Pauli, O. T. Pearce, J. Pearcy, B. Pedrotti, A. Peer, L. J. Pelz, B. Penetrante, J. Penner, A. Perez, L. J. Perkins, E. Pernice, T. S. Perry, S. Person, D. Petersen, T. Petersen, D. L. Peterson, E. B. Peterson, J. E. Peterson, J. L. Peterson, K. Peterson, R. R. Peterson, R. D. Petrasso, F. Philippe, T. J. Phipps, E. Piceno, Y. Ping, L. Pickworth, J. Pino, R. Plummer, G. D. Pollack, S. M. Pollaine, B. B. Pollock, D. Ponce, J. Ponce, J. Pontelandolfo, J. L. Porter, J. Post, O. Poujade, C. Powell, H. Powell, G. Power, M. Pozulp, M. Prantil, M. Prasad, S. Pratuch, S. Price, K. Primdahl, S. Prisbrey, R. Procassini, A. Pruyne, B. Pudliner, S. R. Qiu, K. Quan, M. Quinn, J. Quintenz, P. B. Radha, F. Rainer, J. E. Ralph, K. S. Raman, R. Raman, P. Rambo, S. Rana, A. Randewich, D. Rardin, M. Ratledge, N. Ravelo, F. Ravizza, M. Rayce, A. Raymond, B. Raymond, B. Reed, C. Reed, S. Regan, B. Reichelt, V. Reis, S. Reisdorf, V. Rekow, B. A. Remington, A. Rendon, W. Requieron, M. Rever, H. Reynolds, J. Reynolds, J. Rhodes, M. Rhodes, M. C. Richardson, B. Rice, N. G. Rice, R. Rieben, A. Rigatti, S. Riggs, H. G. Rinderknecht, K. Ring, B. Riordan, R. Riquier, C. Rivers, D. Roberts, V. Roberts, G. Robertson, H. F. Robey, J. Robles, P. Rocha, G. Rochau, J. Rodriguez, S. Rodriguez, M. Rosen, M. Rosenberg, G. Ross, J. S. Ross, P. Ross, J. Rouse, D. Rovang, A. M. Rubenchik, M. S. Rubery, C. L. Ruiz, M. Rushford, B. Russ, J. R. Rygg, B. S. Ryujin, R. A. Sacks, R. F. Sacks, K. Saito, T. Salmon, J. D. Salmonson, J. Sanchez, S. Samuelson, M. Sanchez, C. Sangster, A. Saroyan, J. Sater, A. Satsangi, S. Sauers, S. Saunders, J. P. Sauppe, R. Sawicki, D. Sayre, M. Scanlan, K. Schaffers, G. T. Schappert, S. Schiaffino, D. J. Schlossberg, D. W. Schmidt, M. J. Schmitt, D. H. G. Schneider, M. B. Schneider, R. Schneider, M. Schoff, M. Schollmeier, M. Scholmerich, C. R. Schroeder, S. E. Schrauth, H. A. Scott, I. Scott, J. M. Scott, R. H. H. Scott, C. R. Scullard, T. Sedillo, F. H. Seguin, W. Seka, J. Senecal, S. M. Sepke, L. Seppala, K. Sequoia, J. Severyn, J. M. Sevier, N. Sewell, S. Seznec, R. C. Shah, J. Shamlian, D. Shaughnessy, M. Shaw, R. Shaw, C. Shearer, R. Shelton, N. Shen, M. W. Sherlock, A. I. Shestakov, E. L. Shi, S. J. Shin, N. Shingleton, W. Shmayda, M. Shor, M. Shoup, C. Shuldberg, L. Siegel, F. J. Silva, A. N. Simakov, B. T. Sims, D. Sinars, P. Singh, H. Sio, K. Skulina, S. Skupsky, S. Slutz, M. Sluyter, V. A. Smalyuk, D. Smauley, R. M. Smeltser, C. Smith, I. Smith, J. Smith, L. Smith, R. Smith, R. Sohn, S. Sommer, C. Sorce, M. Sorem, J. M. Soures, M. L. Spaeth, B. K. Spears, S. Speas, D. Speck, R. Speck, J. Spears, T. Spinka, P. T. Springer, M. Stadermann, B. Stahl, J. Stahoviak, L. G. Stanton, R. Steele, W. Steele, D. Steinman, R. Stemke, R. Stephens, S. Sterbenz, P. Sterne, D. Stevens, J. Stevers, C. B. Still, C. Stoeckl, W. Stoeffl, J. S. Stolken, C. Stolz, E. Storm, G. Stone, S. Stoupin, E. Stout, I. Stowers, R. Strauser, H. Streckart, D. J. Strozzi, T. Suratwala, G. Sutcliffe, L. J. Suter, S. B. Sutton, V. Svidzinski, G. Swadling, W. Sweet, A. Szoke, M. Tabak, M. Takagi, A. Tambazidis, V. Tang, M. Taranowski, L. A. Taylor, S. Telford, W. Theobald, M. Thi, A. Thomas, C. A. Thomas, I. Thomas, R. Thomas, I. J. Thompson, A. Thongstisubskul, C. B. Thorsness, G. Tietbohl, R. E. Tipton, M. Tobin, N. Tomlin, R. Tommasini, A. J. Toreja, J. Torres, R. P. J. Town, S. Townsend, J. Trenholme, A. Trivelpiece, C. Trosseille, H. Truax, D. Trummer, S. Trummer, T. Truong, D. Tubbs, E. R. Tubman, T. Tunnell, D. Turnbull, R. E. Turner, M. Ulitsky, R. Upadhye, J. L. Vaher, P. VanArsdall, D. VanBlarcom, M. Vandenboomgaerde, R. VanQuinlan, B. M. Van Wonterghem, W. S. Varnum, A. L. Velikovich, A. Vella, C. P. Verdon, B. Vermillion, S. Vernon, R. Vesey, J. Vickers, R. M. Vignes, M. Visosky, J. Vocke, P. L. Volegov, S. Vonhof, R. Von Rotz, H. X. Vu, M. Vu, D. Wall, J. Wall, R. Wallace, B. Wallin, D. Walmer, C. A. Walsh, C. F. Walters, C. Waltz, A. Wan, A. Wang, Y. Wang, J. S. Wark, B. E. Warner, J. Watson, R. G. Watt, P. Watts, J. Weaver, R. P. Weaver, S. Weaver, C. R. Weber, P. Weber, S. V. Weber, P. Wegner, B. Welday, L. Welser-Sherrill, K. Weiss, K. Widmann, G. F. Wheeler, W. Whistler, R. K. White, H. D. Whitley, P. Whitman, M. E. Wickett, C. Widmayer, J. Wiedwald, R. Wilcox, S. Wilcox, C. Wild, B. H. Wilde, C. H. Wilde, K. Wilhelmsen, M. D. Wilke, H. Wilkens, P. Wilkins, S. C. Wilks, E. A. Williams, G. J. Williams, W. Williams, W. H. Williams, D. C. Wilson, B. Wilson, E. Wilson, R. Wilson, S. Winters, J. Wisoff, M. Wittman, J. Wolfe, A. Wong, K. W. Wong, L. Wong, N. Wong, R. Wood, D. Woodhouse, J. Woodruff, D. T. Woods, S. Woods, B. N. Woodworth, E. Wooten, A. Wootton, K. Work, J. B. Workman, J. Wright, M. Wu, C. Wuest, F. J. Wysocki, H. Xu, M. Yamaguchi, B. Yang, S. T. Yang, J. Yatabe, C. B. Yeamans, B. C. Yee, S. A. Yi, L. Yin, B. Young, C. S. Young, C. V. Young, P. Young, K. Youngblood, R. Zacharias, G. Zagaris, N. Zaitseva, F. Zaka, F. Ze, B. Zeiger, M. Zika, G. B. Zimmerman, T. Zobrist, J. D. Zuegel, A. B. Zylstra, and I.C.F.C. Indirect Drive,

"Lawson criterion for ignition exceeded in an inertial fusion experiment," Phys. Rev. Lett. **129**, 075001 (2022).

[6] Y. Ping, V. A. Smalyuk, P. Amendt, R. Tommasini, J. E. Field, S. Khan, D. Bennett, E. Dewald, F. Graziani, S. Johnson, O. L. Landen, A. G. MacPhee, A. Nikroo, J. Pino, S. Prisbrey, J. Ralph, R. Seugling, D. Strozzi, R. E. Tipton, Y. M. Wang, E. Loomis, E. Merritt, and D. Montgomery, "Enhanced energy coupling for indirectly driven inertial confinement fusion," Nat. Phys. **15**, 138–141 (2019).

[7] Y. Ping, P. Amendt, K. Baker, V. Smalyuk, H. Chen, S. Khan, E. Hartouni, D. Ho, O. Jones, O. Landen, N. Lemos, J. Lindl, J. Moody, A. Nikroo, M. Rubery, D. Schlossberg, M. Stadermann, D. Strozzi, R. Tipton, B. Woodworth, P. Adrian, B. Lahmann, J. Frenje, R. Petrasso, C. Kong, N. Rice, and C. Wild, "Reaching 30% energy coupling efficiency for a high-density-carbon capsule in a gold rugby hohlraum on NIF," Nucl. Fusion **61**, 086028 (2021).

[8] P. Amendt, D. Ho, Y. Ping, V. Smalyuk, S. Khan, J. Lindl, D. Strozzi, R. Tommasini, M. Belyaev, C. Cerjan, O. Jones, W. Kruer, N. Meezan, H. Robey, F. Tsung, C. Weber, and C. Young, "Ultra-high (>30%) coupling efficiency designs for demonstrating central hot-spot ignition on the National Ignition Facility using a frustraum," Phys. Plasmas **26**, 082707 (2019).

[9] G. A. Kyrala, J. L. Kline, S. Dixit, S. Glenzer, D. Kalantar, D. Bradley, N. Izumi, N. Meezan, O. Landen, D. Callahan, S. V. Weber, J. P. Holder, S. Glenn, M. J. Edwards, J. Koch, L. J. Suter, S. W. Haan, R. P. J. Town, P. Michel, O. Jones, S. Langer, J. D. Moody, E. L. Dewald, T. Ma, J. Ralph, A. Hamza, E. Dzenitis, and J. Kilkenny, "Symmetry tuning for ignition capsules via the symcap technique," Phys. Plasmas **18**, 056307 (2011).

[10] G. B. Zimmerman and W. L. Kruer, "Numerical simulation of laser-initiated fusion," Comments Plasma Phys. Controlled Fusion **2**, 51–60 (1975).

[11] P. Michel, L. Divol, E. A. Williams, S. Weber, C. A. Thomas, D. A. Callahan, S. W. Haan, J. D. Salmonson, S. Dixit, D. E. Hinkel, M. J. Edwards, B. J. MacGowan, J. D. Lindl, S. H. Glenzer, and L. J. Suter, "Tuning the implosion symmetry of ICF targets via controlled crossed-beam energy transfer," Phys. Rev. Lett. **102**, 25004 (2009).

[12] J. E. Ralph, P. Michel, B. J. MacGowan, D. J. Strozzi, N. B. Meezan, J. M. Di Nicola, J. E. Heebner, V. J. Hernandez, L. Pelz, S. Yang, N. Lemos, L. Divol, A. Kemp, T. Chapman, S. F. Khan, O. L. Landen, J. D. Moody, R. P. J. Town, and M. J. Edwards, "Optimization of backscatter and symmetry for laser fusion experiments using multiple tunable wavelengths," Phys. Rev. Appl. **18**, 044040 (2022).

[13] D. A. Callahan, O. A. Hurricane, J. E. Ralph, C. A. Thomas, K. L. Baker, L. R. Benedetti, L. F. Berzak Hopkins, D. T. Casey, T. Chapman, C. E. Czajka, E. L. Dewald, L. Divol, T. Döppner, D. E. Hinkel, M. Hohenberger, L. C. Jarrott, S. F. Khan, A. L. Kritcher, O. L. Landen, S. LePape, S. A. MacLaren, L. P. Masse, N. B. Meezan, A. E. Pak, J. D. Salmonson, D. T. Woods, N. Izumi, T. Ma, D. A. Mariscal, S. R. Nagel, J. L. Kline, G. A. Kyrala, E. N. Loomis, S. A. Yi, A. B. Zylstra, and S. H. Batha, "Exploring the limits of case-to-capsule ratio, pulse length, and picket energy for symmetric hohlraum drive on the National Ignition Facility laser," Phys. Plasmas **25**, 056305 (2018).

[14] N. Izumi, D. T. Woods, N. B. Meezan, J. D. Moody, O. L. Landen, L. Divol, H. Chen, D. A. Callahan, M. Hohenberger, A. L. Kritcher, D. T. Casey, M. D. Rosen, J. S. Ross, M. B. Schneider, M. J. Edwards, and W. W. Hsing, "Low mode implosion symmetry sensitivity in low gas-fill NIF cylindrical hohlraums," Phys. Plasmas **28**, 022706 (2021).

[15] O. A. Hurricane and Others, "Extensions of a classical mechanics 'piston-model' for understanding the impact of asymmetry on ICF implosions: The

cases of mode 2, mode 2/1 coupling, time-dependent asymmetry, and the relationship to coast-time," Phys. Plasmas **29**, 12703 (2022).

[16]D. T. Casey, O. L. Landen, E. Hartouni, R. M. Bionta, K. D. Hahn, P. L. Volegov, D. N. Fittinghoff, V. Geppert-Kleinrath, C. H. Wilde, J. L. Milovich, V. A. Smalyuk, J. E. Field, O. A. Hurricane, A. B. Zylstra, A. L. Kritcher, D. S. Clark, C. V. Young, R. C. Nora, D. A. Callahan, B. J. MacGowan, D. H. Munro, B. K. Spears, J. L. Peterson, J. A. Gaffney, K. D. Humbird, M. K. G. Kruse, A. S. Moore, D. J. Schlossberg, M. Gatu-Johnson, and J. A. Frenje, "Three dimensional low-mode areal-density non-uniformities in indirect-drive implosions at the National Ignition Facility," Phys. Plasmas **28**, 042708 (2021).

[17]B. J. MacGowan, O. L. Landen, D. T. Casey, C. V. Young, D. A. Callahan, E. P. Hartouni, R. Hatarik, M. Hohenberger, T. Ma, D. Mariscal, A. Moore, R. Nora, H. G. Rinderknecht, D. Schlossberg, and B. M. Van Wonterghem, "Trending low mode asymmetries in NIF capsule drive using a simple viewfactor metric," High Energy Density Phys. **40**, 100944 (2021).

[18]R. Tommasini, J. E. Field, B. A. Hammel, O. L. Landen, S. W. Haan, C. Aracne-Ruddle, L. R. Benedetti, D. K. Bradley, D. A. Callahan, E. L. Dewald, T. Doeppner, M. J. Edwards, O. A. Hurricane, N. Izumi, O. A. Jones, T. Ma, N. B. Meezan, S. R. Nagel, J. R. Rygg, K. S. Segraves, M. Stadermann, R. J. Strauser, and R. P. J. Town, "Tent-induced perturbations on areal density of implosions at the National Ignition Facility," Phys. Plasmas **22**, 056315 (2015).

[19]S. R. Nagel, S. W. Haan, J. R. Rygg, M. Barrios, L. R. Benedetti, D. K. Bradley, J. E. Field, B. A. Hammel, N. Izumi, O. S. Jones, S. F. Khan, T. Ma, A. E. Pak, R. Tommasini, and R. P. J. Town, "Effect of the mounting membrane on shape in inertial confinement fusion implosions," Phys. Plasmas **22**, 22704 (2015).

[20]V. A. Smalyuk, H. F. Robey, C. L. Alday, P. Amendt, C. Aracne-Ruddle, J. R. Bigelow, T. Bunn, D. T. Casey, K. C. Chen, D. S. Clark, J. P. Cortez, J. Crippen, S. Diaz, M. Farrell, S. Felker, J. E. Field, J. Jaquez, S. Johnson, S. W. Haan, B. A. Hammel, A. V. Hamza, M. O. Havre, C. Heinbockel, W. W. Hsing, K. Kangas, J. J. Kroll, S. O. Kucheyev, O. L. Landen, X. Lepro-Chavez, A. G. MacPhee, D. A. Martinez, J. Milovich, A. Nikroo, L. A. Pickworth, N. Rice, M. Stadermann, D. Steich, and C. R. Weber, "Review of hydro-instability experiments with alternate capsule supports in indirect-drive implosions on the National Ignition Facility," Phys. Plasmas **25**, 072705 (2018).

[21]P. Amendt, D. Ho, O. L. Landen, J. D. Lindl, S. MacLaren, K. L. Baker, D. Mariscal, Y. Ping, J. S. Ross, V. A. Smalyuk, D. J. Strozzi, S. Khan, A. Pak, R. Bionta, D. Casey, P. M. Celliers, D. Fittinghoff, H. Geppert-Kleinrath, V. Geppert-Kleinrath, K. D. Hahn, M. Gat. Johnson, Y. Kim, K. Meaney, M. Millot, P. Volegov, and D. Wilde, "Large-scale capsule implosions on the NIF driven by a frustraum: Modeling comparison using radiation-hydrodynamic simulations," Phys. Plasmas (unpublished).

[22]V. Y. Baranov and O. N. Derkach, "Dynamics and stability of an expanding laser-induced plasma in a low-density gas," Phys. Rev. E **48**, 1324 (1993).

[23]K. L. Baker, C. A. Thomas, T. R. Dittrich, O. Landen, G. Kyrala, D. T. Casey, C. R. Weber, J. Milovich, D. T. Woods, M. Schneider, S. F. Khan, B. K. Spears, A. Zylstra, C. Kong, J. Crippen, N. Alfonso, C. B. Yeamans, J. D. Moody, A. S. Moore, N. B. Meezan, A. Pak, D. N. Fittinghoff, P. L. Volegov, O. Hurricane, D. Callahan, P. Patel, and P. Amendt, "Fill tube dynamics in inertial confinement fusion implosions with high density carbon ablators," Phys. Plasmas **27**, 112706 (2020).

[24]B. R. Munson, D. F. Young, and T. H. Okiishi, *Fundamentals of Fluid Mechanics*, 3rd ed. (John Wiley and Sons, Inc., 1998).

[25]T. Ma, P. K. Patel, N. Izumi, P. T. Springer, M. H. Key, L. J. Atherton, L. R. Benedetti, D. K. Bradley, D. A. Callahan, P. M. Celliers, C. J. Cerjan, D. S. Clark, E. L. Dewald, S. N. Dixit, T. Döppner, D. H. Edgell, R. Epstein, S. Glenn, G. Grim, S. W. Haan, B. A. Hammel, D. Hicks, W. W. Hsing, O. S. Jones, S. F. Khan, J. D. Kilkenny, J. L. Kline, G. A. Kyrala, O. L. Landen, S. Le Pape, B. J. Macgowan, A. J. Mackinnon, A. G. Macphee, N. B. Meezan, J. D. Moody, A. Pak, T. Parham, H.-S. Park, J. E. Ralph, S. P. Regan, B. A. Remington, H. F. Robey, J. S. Ross, B. K. Spears, V. Smalyuk, L. J. Suter, R. Tommasini, R. P. Town, S. V. Weber, J. D. Lindl, M. J. Edwards, S. H. Glenzer, and E. I. Moses, "Onset of hydrodynamic mix in high-velocity, highly compressed inertial confinement fusion implosions," Phys. Rev. Lett. **111**, 085004 (2013).

[26]B. M. Haines, R. C. Shah, J. M. Smidt, B. J. Albright, T. Cardenas, M. R. Douglas, C. Forrest, V. Y. Glebov, M. A. Gunderson, C. E. Hamilton, K. C. Henderson, Y. Kim, M. N. Lee, T. J. Murphy, J. A. Oertel, R. E. Olson, B. M. Patterson, R. B. Randolph, and D. W. Schmidt, "Observation of persistent species temperature separation in inertial confinement fusion mixtures," Nat. Commun. **11**, 544 (2020).

[27]K. Baker, C. Thomas, O. Landen, S. Haan, J. Lindl, D. Casey, C. Young, R. Nora, O. Hurricane, D. Callahan, O. Jones, L. Berzak Hopkins, S. Khan, B. Spears, S. Le Pape, N. Meezan, D. Ho, T. Döppner, D. Hinkel, E. Dewald, R. Tommasini, M. Hohenberger, C. Weber, D. Clark, D. Woods, J. Milovich, D. Strozzi, A. Kritcher, H. Robey, J. Ross, V. Smalyuk, P. Amendt, B. Bachmann, L. Benedetti, R. Bionta, P. Celliers, D. Fittinghoff, C. Goyon, R. Hatarik, N. Izumi, M. Gatu Johnson, G. Kyrala, T. Ma, K. Meaney, M. Millot, S. Nagel, P. Patel, D. Turnbull, P. Volegov, C. Yeamans, and B. H. Wilde, "Reaching a burning plasma and ignition using smaller capsules/hohlraums, higher radiation temperatures, and thicker ablator/ice on the National Ignition Facility," Phys. Plasmas **30**, 032702 (2023).

[28]K. L. Baker, C. A. Thomas, D. T. Casey, S. Khan, B. K. Spears, R. Nora, T. Woods, J. L. Milovich, R. L. Berger, D. Strozzi, D. Clark, M. Hohenberger, O. A. Hurricane, D. A. Callahan, O. L. Landen, B. Bachmann, R. Benedetti, R. Bionta, P. M. Celliers, D. Fittinghoff, C. Goyon, G. Grim, R. Hatarik, N. Izumi, M. Gatu Johnson, G. Kyrala, T. Ma, M. Millot, S. R. Nagel, A. Pak, P. K. Patel, D. Turnbull, P. L. Volegov, and C. Yeamans, "High-performance indirect-drive cryogenic implosions at high adiabat on the National Ignition Facility," Phys. Rev. Lett. **121**, 135001 (2018).

[29]K. L. Baker, *Improved Stagnation Pressure* (LLNL, 2019).

[30]K. L. Baker, S. MacLaren, O. Jones, B. K. Spears, P. K. Patel, R. Nora, L. Divol, O. L. Landen, G. J. Anderson, J. Gaffney, M. Kruse, O. A. Hurricane, D. A. Callahan, A. R. Christopherson, J. Salmonson, E. P. Hartouni, T. Döppner, E. Dewald, R. Tommasini, C. A. Thomas, C. Weber, D. Clark, D. T. Casey, M. Hohenberger, S. Khan, T. Woods, J. L. Milovich, R. L. Berger, D. Strozzi, A. Kritcher, B. Bachmann, R. Benedetti, R. Bionta, P. M. Celliers, D. Fittinghoff, R. Hatarik, N. Izumi, M. Gatu Johnson, G. Kyrala, T. Ma, K. Meaney, M. Millot, S. R. Nagel, A. Pak, P. L. Volegov, C. Yeamans, and C. Wilde, "Alpha heating of indirect-drive layered implosions on the National Ignition Facility," Phys. Rev. E **107**, 015202 (2023).

[31]K. L. Baker, C. A. Thomas, D. T. Casey, M. Hohenberger, S. Khan, B. K. Spears, O. L. Landen, R. Nora, D. T. Woods, J. L. Milovich, R. L. Berger, D. Strozzi, C. Weber, D. Clark, O. A. Hurricane, D. A. Callahan, A. L. Kritcher, B. Bachmann, L. R. Benedetti, R. Bionta, P. M. Celliers, D. Fittinghoff, C. Goyon, R. Hatarik, N. Izumi, M. Gatu Johnson, G. Kyrala, T. Ma, K. Meaney, M. Millot, S. R. Nagel, P. K. Patel, D. Turnbull, P. L. Volegov, C. Yeamans, and C. Wilde, "Hotspot parameter scaling with velocity and yield for high-adiabat layered implosions at the National Ignition Facility," Phys. Rev. E **102**, 023210 (2020).

[32]P. K. Patel, P. T. Springer, C. R. Weber, L. C. Jarrott, O. A. Hurricane, B. Bachmann, K. L. Baker, L. F. Berzak Hopkins, D. A. Callahan, D. T. Casey, C. J. Cerjan, D. S. Clark, E. L. Dewald, L. Divol, T. Döppner, J. E. Field, D. Fittinghoff, J. Gaffney, V. Geppert-Kleinrath, G. P. Grim, E. P. Hartouni, R. Hatarik, D. E. Hinkel, M. Hohenberger, K. Humbird, N. Izumi, O. S. Jones, S. F. Khan, A. L. Kritcher, M. Kruse, O. L. Landen, S. Le Pape, T. Ma, S. A. MacLaren, A. G. MacPhee, L. P. Masse, N. B. Meezan, J. L. Milovich, R. Nora, A. Pak, J. L. Peterson, J. Ralph, H. F. Robey, J. D. Salmonson, V. A. Smalyuk, B. K. Spears, C. A. Thomas, P. L. Volegov, A. Zylstra, and M. J. Edwards, "Hotspot conditions achieved in inertial confinement fusion experiments on the National Ignition Facility," Phys. Plasmas **27**, 050901 (2020).

[33]D. T. Casey, C. A. Thomas, K. L. Baker, B. K. Spears, M. Hohenberger, S. F. Khan, R. C. Nora, C. R. Weber, D. T. Woods, O. A. Hurricane, D. A. Callahan, R. L. Berger, J. L. Milovich, P. K. Patel, T. Ma, A. Pak, L. R. Benedetti, M. Millot, C. Jarrott, O. L. Landen, R. M. Bionta, B. J. MacGowan, D. J. Strozzi, M. Stadermann, J. Biener, A. Nikroo, C. S. Goyon, N. Izumi, S. R. Nagel, B. Bachmann, P. L. Volegov, D. N. Fittinghoff, G. P. Grim, C. B. Yeamans, M. Gatu Johnson, J. A. Frenje, N. Rice, C. Kong, J. Crippen, J. Jaquez, K. Kangas, and C. Wild, "The high velocity, high adiabat, 'Bigfoot' campaign and tests of indirect-drive implosion scaling," Phys. Plasmas **25**, 056308 (2018).

[34]C. A. Thomas, E. M. Campbell, K. L. Baker, D. T. Casey, M. Hohenberger, A. L. Kritcher, B. K. Spears, S. F. Khan, R. Nora, D. T. Woods, J. L. Milovich, R. L. Berger, D. Strozzi, D. D. Ho, D. Clark, B. Bachmann, L. R. Benedetti, R. Bionta, P. M. Celliers, D. N. Fittinghoff, G. Grim, R. Hatarik, N. Izumi, G. Kyrala, T. Ma, M. Millot, S. R. Nagel, P. K. Patel, C. Yeamans, A. Nikroo, M. Tabak, M.

28 September 2023 14:55:57

Gatu Johnson, P. L. Volegov, and S. M. Finnegan, "Deficiencies in compression and yield in x-ray-driven implosions," Phys. Plasmas **27**, 112705 (2020).

[35]C. A. Thomas, E. M. Campbell, K. L. Baker, D. T. Casey, M. Hohenberger, A. L. Kritcher, B. K. Spears, S. F. Khan, R. Nora, D. T. Woods, J. L. Milovich, R. L. Berger, D. Strozzi, D. D. Ho, D. Clark, B. Bachmann, L. R. Benedetti, R. Bionta, P. M. Celliers, D. N. Fittinghoff, G. Grim, R. Hatarik, N. Izumi, G. Kyrala, T. Ma, M. Millot, S. R. Nagel, P. K. Patel, C. Yeamans, A. Nikroo, M. Tabak, M. Gatu Johnson, P. L. Volegov, and S. M. Finnegan, "Principal factors in performance of indirect-drive laser fusion experiments," Phys. Plasmas **27**, 112712 (2020).

[36]C. A. Thomas, E. M. Campbell, K. L. Baker, D. T. Casey, M. Hohenberger, A. L. Kritcher, B. K. Spears, S. F. Khan, R. Nora, D. T. Woods, J. L. Milovich, R. L. Berger, D. Strozzi, D. D. Ho, D. Clark, B. Bachmann, L. R. Benedetti, R. Bionta, P. M. Celliers, D. N. Fittinghoff, G. Grim, R. Hatarik, N. Izumi, G. Kyrala, T. Ma, M. Millot, S. R. Nagel, P. K. Patel, C. Yeamans, A. Nikroo, M. Tabak, M. G. Johnson, P. L. Volegov, and S. M. Finnegan, "Experiments to explore the influence of pulse shaping at the National Ignition Facility," Phys. Plasmas **27**, 112708 (2020).

[37]M. Hohenberger, D. T. Casey, C. A. Thomas, O. L. Landen, K. L. Baker, L. R. Benedetti, D. A. Callahan, O. A. Hurricane, N. Izumi, S. F. Khan, T. Ma, D. A. Mariscal, S. R. Nagel, A. Pak, and B. K. Spears, "Maintaining low-mode symmetry control with extended pulse shapes for lower-adiabat Bigfoot implosions on the National Ignition Facility," Phys. Plasmas **26**, 112707 (2019).

[38]R. Berger, C. A. Thomas, K. Baker, D. Casey, C. Goyon, J. Park, N. Lemos, S. Khan, M. Hohenberger, J. Milovich, D. Strozzi, M. Belyaev, T. Chapman, and A. B. Langdon, "Stimulated backscatter of laser light from bigfoot hohlraums on the National Ignition Facility," Phys. Plasmas **26**, 012709 (2019).

[39]H. F. Robey, P. M. Celliers, J. L. Kline, A. J. Mackinnon, T. R. Boehly, O. L. Landen, J. H. Eggert, D. Hicks, S. L. Pape, D. R. Farley, M. W. Bowers, K. G. Krauter, D. H. Munro, O. S. Jones, J. L. Milovich, D. Clark, B. K. Spears, R. P. J. Town, S. W. Haan, S. Dixit, M. B. Schneider, E. L. Dewald, K. Widmann, J. D. Moody, T. Döppner, H. B. Radousky, A. Nikroo, J. J. Kroll, A. V. Hamza, J. B. Horner, S. D. Bhandarkar, E. Dzenitis, E. Alger, E. Giraldez, C. Castro, K. Moreno, C. Haynam, K. N. Lafortune, C. Widmayer, M. Shaw, K. Jancaitis, T. Parham, D. M. Holunga, C. F. Walters, B. Haid, T. Malsbury, D. Trummer, K. R. Coffee, B. Burr, L. V. Berzins, C. Choate, S. J. Brereton, S. Azevedo, H. Chandrasekaran, S. Glenzer, J. A. Caggiano, J. P. Knauer, J. A. Frenje, D. T. Casey, M. G. Johnson, F. H. Séguin, B. K. Young, M. J. Edwards, B. M. Van Wonterghem, J. Kilkenny, B. J. Macgowan, L. J. Atherton, J. D. Lindl, D. D. Meyerhofer, and E. Moses, "Shock timing on the National Ignition Facility: The first precision tuning series," EPJ Web Conf. **59**, 02005 (2013).

[40]V. A. Smalyuk, L. J. Atherton, L. R. Benedetti, R. Bionta, D. Bleuel, E. Bond, D. K. Bradley, J. Caggiano, D. A. Callahan, D. T. Casey, P. M. Celliers, C. J. Cerjan, D. Clark, E. L. Dewald, S. N. Dixit, T. Doppner, D. H. Edgell, M. J. Edwards, J. Frenje, M. Gatu-Johnson, V. Y. Glebov, S. Glenn, S. H. Glenzer, G. Grim, S. W. Haan, B. A. Hammel, E. P. Hartouni, R. Hatarik, S. Hatchett, D. G. Hicks, W. W. Hsing, N. Izumi, O. S. Jones, M. H. Key, S. F. Khan, J. D. Kilkenny, J. L. Kline, J. Knauer, G. A. Kyrala, O. L. Landen, S. Le Pape, J. D. Lindl, T. Ma, B. J. MacGowan, A. J. Mackinnon, A. G. MacPhee, J. McNaney, N. B. Meezan, J. D. Moody, A. Moore, M. Moran, E. I. Moses, A. Pak, T. Parham, H. S. Park, P. K. Patel, R. Petrasso, J. E. Ralph, S. P. Regan, B. A. Remington, H. F. Robey, J. S. Ross, B. K. Spears, P. T. Springer, L. J. Suter, R. Tommasini, R. P. Town, S. V. Weber, and K. Widmann, "Performance of high-convergence, layered DT implosions with extended-duration pulses at the National Ignition Facility," Phys. Rev. Lett. **111**, 215001 (2013).

[41]O. L. Landen, R. Benedetti, D. Bleuel, T. R. Boehly, D. K. Bradley, J. A. Caggiano, D. A. Callahan, P. M. Celliers, C. J. Cerjan, D. Clark, G. W. Collins, E. L. Dewald, S. N. Dixit, T. Doeppner, D. Edgell, J. Eggert, D. Farley, J. A. Frenje, V. Glebov, S. M. Glenn, S. H. Glenzer, S. W. Haan, A. Hamza, B. A. Hammel, C. A. Haynam, J. H. Hammer, R. F. Heeter, H. W. Herrmann, D. G. Hicks, D. E. Hinkel, N. Izumi, M. Gatu Johnson, O. S. Jones, D. H. Kalantar, R. L. Kauffman, J. D. Kilkenny, J. L. Kline, J. P. Knauer, J. A. Koch, G. A. Kyrala, K. LaFortune, T. Ma, A. J. Mackinnon, A. J. Macphee, E. Mapoles, J. L. Milovich, J. D. Moody, N. B. Meezan, P. Michel, A. S. Moore, D. H. Munro, A. Nikroo, R. E. Olson, K. Opachich, A. Pak, T. Parham, P. Patel, H. S. Park, R. P. Petrasso, J. Ralph, S. P. Regan, B. A. Remington, H. G. Rinderknecht, H. F. Robey, M. D. Rosen, J. S. Ross, J. D. Salmonson, T. C. Sangster, M. B.

Schneider, V. Smalyuk, B. K. Spears, P. T. Springer, L. J. Suter, C. A. Thomas, R. P. J. Town, S. V. Weber, P. J. Wegner, D. C. Wilson, K. Widmann, C. Yeamans, A. Zylstra, M. J. Edwards, J. D. Lindl, L. J. Atherton, W. W. Hsing, B. J. MacGowan, B. M. Van Wonterghem, and E. I. Moses, "Progress in the indirect-drive National Ignition Facility," Plasma Phys. Controlled Fusion **54**, 124026 (2012).

[42]O. L. Landen, D. T. Casey, J. M. DiNicola, T. Doeppner, E. P. Hartouni, D. E. Hinkel, L. F. Berzak Hopkins, M. Hohenberger, A. L. Kritcher, S. LePape, B. J. MacGowan, S. Maclaren, K. D. Meaney, M. Millot, P. K. Patel, J. Park, L. A. Pickworth, H. F. Robey, J. S. Ross, S. T. Yang, A. B. Zylstra, K. L. Baker, D. A. Callahan, P. M. Celliers, M. J. Edwards, O. A. Hurricane, J. D. Lindl, J. D. Moody, J. Ralph, V. A. Smalyuk, C. A. Thomas, B. M. Van Wonterghem, and C. R. Weber, "Yield and compression trends and reproducibility at NIF," High Energy Density Phys. **36**, 100765 (2020).

[43]O. A. Hurricane, A. Kritcher, D. A. Callahan, O. Landen, P. K. Patel, P. T. Springer, D. T. Casey, E. L. Dewald, T. R. Dittrich, T. Döppner, D. E. Hinkel, L. F. Berzak Hopkins, J. Kline, S. Le Pape, T. Ma, A. G. MacPhee, A. Moore, A. Pak, H. S. Park, J. Ralph, J. D. Salmonson, and K. Widmann, "On the importance of minimizing 'coast-time' in x-ray driven inertially confined fusion implosions," Phys. Plasmas **24**, 092706 (2017).

[44]J. D. Moody, O. L. Landen, L. Divol, S. LePape, P. Michel, R. P. J. Town, G. Hall, K. Widmann, and A. Moore, "Semi-empirical 'leaky-bucket' model of laser-driven x-ray cavities," Phys. Plasmas **24**, 042709 (2017).

[45]J. D. Lindl, P. Amendt, R. L. Berger, S. G. Glendinning, S. H. Glenzer, S. W. Haan, R. L. Kauffman, O. L. Landen, and L. J. Suter, "The physics basis for ignition using indirect-drive targets on the National Ignition Facility," Phys. Plasmas **11**, 339–491 (2004).

[46]J. D. Lindl, private communication (2023).

[47]M. Basko, "An improved version of the view factor method for simulating inertial confinement fusion hohlraums," Phys. Plasmas **3**, 4148–4155 (1996).

[48]M. D. Rosen, "Analytic modeling of hohlraum drive for high performing HDC capsules," in *Proceedings of the 63rd Annual Meeting of the APS Division of Plasma Physics* (American Institute of Physics for the American Physical Society, Pittsburgh, PA, 2021).

[49]J. Schein, O. Jones, M. Rosen, E. Dewald, S. Glenzer, J. Gunther, B. Hammel, O. Landen, L. Suter, and R. Wallace, "Demonstration of enhanced radiation drive in hohlraums made from a mixture of high-Z wall materials," Phys. Rev. Lett. **98**, 175003 (2007).

[50]A. J. MacKinnon, N. B. Meezan, J. S. Ross, S. L. Pape, L. Berzak Hopkins, L. Divol, D. Ho, J. Milovich, A. Pak, J. Ralph, T. Döppner, P. K. Patel, C. Thomas, R. Tommasini, S. Haan, A. G. MacPhee, J. McNaney, J. Caggiano, R. Hatarik, R. Bionta, T. Ma, B. Spears, J. R. Rygg, L. R. Benedetti, R. P. J. Town, D. K. Bradley, E. L. Dewald, D. Fittinghoff, O. S. Jones, H. R. Robey, J. D. Moody, S. Khan, D. A. Callahan, A. Hamza, J. Biener, P. M. Celliers, D. G. Braun, D. J. Erskine, S. T. Prisbrey, R. J. Wallace, B. Kozioziemski, R. Dylla-Spears, J. Sater, G. Collins, E. Storm, W. Hsing, O. Landen, J. L. Atherton, J. D. Lindl, M. J. Edwards, J. A. Frenje, M. Gatu-Johnson, C. K. Li, R. Petrasso, H. Rinderknecht, M. Rosenberg, F. H. Séguin, A. Zylstra, J. P. Knauer, G. Grim, N. Guler, F. Merrill, R. Olson, G. A. Kyrala, J. D. Kilkenny, A. Nikroo, K. Moreno, D. E. Hoover, C. Wild, and E. Werner, "High-density carbon ablator experiments on the National Ignition Facility," Phys. Plasmas **21**, 056318 (2014).

[51]S. L. Pape, L. F. Berzak Hopkins, L. Divol, A. Pak, E. L. Dewald, S. Bhandarkar, L. R. Bennedetti, T. Bunn, J. Biener, J. Crippen, D. Casey, D. Edgell, D. N. Fittinghoff, M. Gatu-Johnson, C. Goyon, S. Haan, R. Hatarik, M. Havre, D. D. Ho, N. Izumi, J. Jaquez, S. F. Khan, G. A. Kyrala, T. Ma, A. J. Mackinnon, A. G. MacPhee, B. J. MacGowan, N. B. Meezan, J. Milovich, M. Millot, P. Michel, S. R. Nagel, A. Nikroo, P. Patel, J. Ralph, J. S. Ross, N. G. Rice, D. Strozzi, M. Stadermann, P. Volegov, C. Yeamans, C. Weber, C. Wild, D. Callahan, and O. A. Hurricane, "Fusion energy output greater than the kinetic energy of an imploding shell at the National Ignition Facility," Phys. Rev. Lett. **120**, 245003 (2018).

[52]L. F. Berzak Hopkins, N. B. Meezan, S. Le Pape, L. Divol, A. J. Mackinnon, D. D. Ho, M. Hohenberger, O. S. Jones, G. Kyrala, J. L. Milovich, A. Pak, J. E. Ralph, J. S. Ross, L. R. Benedetti, J. Biener, R. Bionta, E. Bond, D. Bradley, J. Caggiano, D. Callahan, C. Cerjan, J. Church, D. Clark, T. Doppner, R. Dylla-Spears, M. Eckart, D. Edgell, J. Field, D. N. Fittinghoff, M. Gatu Johnson, G.

Grim, N. Guler, S. Haan, A. Hamza, E. P. Hartouni, R. Hatarik, H. W. Herrmann, D. Hinkel, D. Hoover, H. Huang, N. Izumi, S. Khan, B. Kozioziemski, J. Kroll, T. Ma, A. MacPhee, J. McNaney, F. Merrill, J. Moody, A. Nikroo, P. Patel, H. F. Robey, J. R. Rygg, J. Sater, D. Sayre, M. Schneider, S. Sepke, M. Stadermann, W. Stoeffl, C. Thomas, R. P. Town, P. L. Volegov, C. Wild, C. Wilde, E. Woerner, C. Yeamans, B. Yoxall, J. Kilkenny, O. L. Landen, W. Hsing, and M. J. Edwards, "First high-convergence cryogenic implosion in a near-vacuum hohlraum," Phys. Rev. Lett. **114**, 175001 (2015).

[53] N. B. Meezan, L. F. Berzak Hopkins, S. L. Pape, L. Divol, A. J. MacKinnon, T. Döppner, D. D. Ho, O. S. Jones, S. F. Khan, T. Ma, J. L. Milovich, A. E. Pak, J. S. Ross, C. A. Thomas, L. R. Benedetti, D. K. Bradley, P. M. Celliers, D. S. Clark, J. E. Field, S. W. Haan, N. Izumi, G. A. Kyrala, J. D. Moody, P. K. Patel, J. E. Ralph, J. R. Rygg, S. M. Sepke, B. K. Spears, R. Tommasini, R. P. J. Town, J. Biener, R. M. Bionta, E. J. Bond, J. A. Caggiano, M. J. Eckart, M. Gatu Johnson, G. P. Grim, A. V. Hamza, E. P. Hartouni, R. Hatarik, D. E. Hoover, J. D. Kilkenny, B. J. Kozioziemski, J. J. Kroll, J. M. McNaney, A. Nikroo, D. B. Sayre, M. Stadermann, C. Wild, B. E. Yoxall, O. L. Landen, W. W. Hsing, and M. J. Edwards, "Cryogenic tritium-hydrogen-deuterium and deuterium-tritium layer implosions with high density carbon ablators in near-vacuum hohlraums," Phys. Plasmas **22**, 062703 (2015).

[54] D. D. M. Ho, S. W. Haan, J. D. Salmonson, D. S. Clark, J. D. Lindl, J. L. Milovich, C. A. Thomas, L. F. Berzak Hopkins, and N. B. Meezan, "Implosion configurations for robust ignition using high-density carbon (diamond) ablator for indirect-drive ICF at the National Ignition Facility," J. Phys.: Conf. Ser. **717**, 012023 (2016).

[55] L. Divol, A. Pak, L. F. Berzak Hopkins, S. L. Pape, N. B. Meezan, E. L. Dewald, D. D. M. Ho, S. F. Khan, A. J. Mackinnon, J. S. Ross, D. P. Turnbull, C. Weber, P. M. Celliers, M. Millot, L. R. Benedetti, J. E. Field, N. Izumi, G. A. Kyrala, T. Ma, S. R. Nagel, J. R. Rygg, D. Edgell, A. G. Macphee, C. Goyon, M. Hohenberger, B. J. MacGowan, P. Michel, D. Strozzi, W. S. Cassata, D. Casey, D. N. Fittinghoff, N. Gharibyan, R. Hatarik, D. Sayre, P. Volegov, C. Yeamans, B. Bachmann, T. Döppner, J. Biener, J. Crippen, C. Choate, H. Huang, C. Kong, A. Nikroo, N. G. Rice, M. Stadermann, S. D. Bhandarkar, S. Haan, B. Kozioziemski, W. W. Hsing, O. L. Landen, J. D. Moody, R. P. J. Town, D. A. Callahan, O. A. Hurricane, and M. J. Edwards, "Symmetry control of an indirectly driven high-density-carbon implosion at high convergence and high velocity," Phys. Plasmas **24**, 056309 (2017).

[56] A. L. Kritcher, C. Young, H. F. Robey, and Others, "Design of implosions reaching the burning plasma regime," Nat. Phys. **18**, 251–258 (2022).

[57] H. F. Robey, L. Berzak Hopkins, J. L. Milovich, and N. B. Meezan, "The I-Raum: A new shaped hohlraum for improved inner beam propagation in indirectly-driven ICF implosions on the National Ignition Facility," Phys. Plasmas **25**, 012711 (2018).

[58] M. Hohenberger, D. T. Casey, A. L. Kritcher, A. Pak, A. B. Zylstra, C. A. Thomas, K. L. Baker, S. Le Pape, B. Bachmann, R. L. Berger, J. Biener, D. S. Clark, L. Divol, T. Döppner, V. Geppert-Kleinrath, D. Hinkel, H. Huang, C. Kong, O. L. Landen, J. Milovich, A. Nikroo, N. Rice, H. Robey, M. Schoff, J. Sevier, K. Sequoia, M. Stadermann, D. Strozzi, P. L. Volegov, C. Weber, C. Wild, B. Woodworth, D. A. Callahan, and O. A. Hurricane, "Integrated performance of large HDC-capsule implosions on the National Ignition Facility," Phys. Plasmas **27**, 112704 (2020).

[59] A. B. Zylstra, A. L. Kritcher, O. A. Hurricane, D. A. Callahan, K. Baker, T. Braun, D. T. Casey, D. Clark, K. Clark, T. Doppner, L. Divol, D. E. Hinkel, M. Hohenberger, C. Kong, O. L. Landen, A. Nikroo, A. Pak, P. Patel, J. E. Ralph, N. Rice, R. Tommasini, M. Schoff, M. Stadermann, D. Strozzi, C. Weber, C. Young, C. Wild, R. P. J. Town, and M. J. Edwards, "Record energetics for an inertial fusion implosion at NIF," Phys. Rev. Lett. **126**, 025001 (2021).

[60] A. L. Kritcher, A. B. Zylstra, D. A. Callahan, O. A. Hurricane, C. Weber, J. Ralph, D. T. Casey, A. Pak, K. Baker, B. Bachmann, S. Bhandarkar, J. Biener, R. Bionta, T. Braun, M. Bruhn, C. Choate, D. Clark, J. M. Di Nicola, L. Divol, T. Doeppner, V. Geppert-Kleinrath, S. Haan, J. Heebner, V. Hernandez, D. Hinkel, M. Hohenberger, H. Huang, C. Kong, S. L. Pape, D. Mariscal, E.

Marley, L. Masse, K. D. Meaney, M. Millot, A. Moore, K. Newman, A. Nikroo, P. Patel, L. Pelz, N. Rice, H. Robey, J. S. Ross, M. Rubery, J. Salmonson, D. Schlossberg, S. Sepke, K. Sequoia, M. Stadermann, D. Strozzi, R. Tommasini, P. Volegov, C. Wild, S. Yang, C. Young, M. J. Edwards, O. Landen, R. Town, and M. Herrmann, "Achieving record hot spot energies with large HDC implosions on NIF in HYBRID-E," Phys. Plasmas **28**, 072706 (2021).

[61] A. B. Zylstra, A. L. Kritcher, O. A. Hurricane, D. A. Callahan, J. E. Ralph, D. T. Casey, A. Pak, O. L. Landen, B. Bachmann, K. L. Baker, L. Berzak Hopkins, S. D. Bhandarkar, J. Biener, R. M. Bionta, N. W. Birge, T. Braun, T. M. Briggs, P. M. Celliers, H. Chen, C. Choate, D. S. Clark, L. Divol, T. Döppner, D. Fittinghoff, M. J. Edwards, M. Gatu Johnson, N. Gharibyan, S. Haan, K. D. Hahn, E. Hartouni, D. E. Hinkel, D. D. Ho, M. Hohenberger, J. P. Holder, H. Huang, N. Izumi, J. Jeet, O. Jones, S. M. Kerr, S. F. Khan, H. Geppert Kleinrath, V. Geppert Kleinrath, C. Kong, K. M. Lamb, S. L. Pape, N. C. Lemos, J. D. Lindl, B. J. MacGowan, A. J. Mackinnon, A. G. MacPhee, E. V. Marley, K. Meaney, M. Millot, A. S. Moore, K. Newman, J. M. G. Di Nicola, A. Nikroo, R. Nora, P. K. Patel, N. G. Rice, M. S. Rubery, J. Sater, D. J. Schlossberg, S. M. Sepke, K. Sequoia, S. J. Shin, M. Stadermann, S. Stoupin, D. J. Strozzi, C. A. Thomas, R. Tommasini, C. Trosseille, E. R. Tubman, P. L. Volegov, C. R. Weber, C. Wild, D. T. Woods, S. T. Yang, and C. V. Young, "Experimental achievement and signatures of ignition at the National Ignition Facility," Phys. Rev. E **106**, 025202 (2022).

[62] A. L. Kritcher, A. B. Zylstra, D. A. Callahan, O. A. Hurricane, C. R. Weber, D. S. Clark, C. V. Young, J. E. Ralph, D. T. Casey, A. Pak, O. L. Landen, B. Bachmann, K. L. Baker, L. Berzak Hopkins, S. D. Bhandarkar, J. Biener, R. M. Bionta, N. W. Birge, T. Braun, T. M. Briggs, P. M. Celliers, H. Chen, C. Choate, L. Divol, T. Döppner, D. Fittinghoff, M. J. Edwards, M. Gatu Johnson, N. Gharibyan, S. Haan, K. D. Hahn, E. Hartouni, D. E. Hinkel, D. D. Ho, M. Hohenberger, J. P. Holder, H. Huang, N. Izumi, J. Jeet, O. Jones, S. M. Kerr, S. F. Khan, H. Geppert Kleinrath, V. Geppert Kleinrath, C. Kong, K. M. Lamb, S. L. Pape, N. C. Lemos, J. D. Lindl, B. J. MacGowan, A. J. Mackinnon, A. G. MacPhee, E. V. Marley, K. Meaney, M. Millot, A. S. Moore, K. Newman, J. M. G. Di Nicola, A. Nikroo, R. Nora, P. K. Patel, N. G. Rice, M. S. Rubery, J. Sater, D. J. Schlossberg, S. M. Sepke, K. Sequoia, S. J. Shin, M. Stadermann, S. Stoupin, D. J. Strozzi, C. A. Thomas, R. Tommasini, C. Trosseille, E. R. Tubman, P. L. Volegov, C. Wild, D. T. Woods, and S. T. Yang, "Design of an inertial fusion experiment exceeding the Lawson criterion for ignition," Phys. Rev. E **106**, 025201 (2022).

[63] R. Tommasini, D. T. Casey, D. Clark, A. Do, K. L. Baker, O. L. Landen, V. A. Smalyuk, C. Weber, B. Bachmann, E. Hartouni, E. V. Marley, M. Millot, J. Milovich, R. C. Nora, A. E. Pak, D. Schlossberg, B. Woodworth, T. M. Briggs, D. M. Holunga, A. Nikroo, and M. Stadermann, "Increased compression in HDC-based ablator implosions using modified drive profile," Phys. Rev. Res. (submitted) (2023).

[64] O. L. Landen, J. D. Lindl, S. W. Haan, D. T. Casey, P. M. Celliers, D. N. Fittinghoff, N. Gharibyan, V. N. Goncharov, G. P. Grim, E. P. Hartouni, O. A. Hurricane, B. J. MacGowan, S. A. MacLaren, K. D. Meaney, M. Millot, J. L. Milovich, P. K. Patel, H. S. Robey, P. T. Springer, P. L. Volegov, and M. J. Edwards, "Fuel convergence sensitivity in indirect drive implosions," Phys. Plasmas **28**, 042705 (2021).

[65] J. D. Lindl, S. W. Haan, and O. L. Landen, "Impact of hohlraum cooling on ignition metrics for inertial fusion implosions," Phys. Plasmas **30**, 012705 (2023).

[66] J. D. Lindl, S. W. Haan, O. L. Landen, A. R. Christopherson, and R. Betti, "Progress toward a self-consistent set of 1D ignition capsule metrics in ICF," Phys. Plasmas **25**, 122704 (2018).

[67] J. A. Koch, "Volume and surface area of a spherical harmonic surface approximation to a NIF implosion core defined by HGXI/GXD images from the equator and pole," Report No. LLNL-TR-510411 (LLNL, 2011).

[68] B. Cheng, T. J. T. Kwan, S. A. Yi, O. L. Landen, Y. M. Wang, C. J. Cerjan, S. H. Batha, and F. J. Wysocki, "Effects of asymmetry and hot-spot shape on ignition capsules," Phys. Rev. E **98**, 023203 (2018).